

Experimental Test of High-Dimensional Quantum Contextuality Based on Contextuality Concentration

Zheng-Hao Liu,^{1,2,*} Hui-Xian Meng,^{3,4} Zhen-Peng Xu,⁵ Jie Zhou,^{4,6} Jing-Ling Chen,^{4,†}
Jin-Shi Xu,^{1,2,7,‡} Chuan-Feng Li,^{1,2,7,§} Guang-Can Guo,^{1,2,7} and Adán Cabello^{8,9,¶}

¹*CAS Key Laboratory of Quantum Information, University of Science and Technology of China, Hefei 230026, People's Republic of China*

²*CAS Centre For Excellence in Quantum Information and Quantum Physics, University of Science and Technology of China, Hefei 230026, People's Republic of China*

³*School of Mathematics and Physics, North China Electric Power University, Beijing 102206, People's Republic of China*

⁴*Theoretical Physics Division, Chern Institute of Mathematics, Nankai University, Tianjin 300071, People's Republic of China*

⁵*Naturwissenschaftlich-Technische Fakultät, Universität Siegen, Walter-Flex-Straße 3, 57068 Siegen, Germany*

⁶*Centre for Quantum Technologies, National University of Singapore 117543, Singapore*

⁷*Hefei National Laboratory, University of Science and Technology of China, Hefei 230088, People's Republic of China*

⁸*Departamento de Física Aplicada II, Universidad de Sevilla, E-41012 Sevilla, Spain*

⁹*Instituto Carlos I de Física Teórica y Computacional, Universidad de Sevilla, E-41012 Sevilla, Spain*
(Dated: April 5, 2023)

Contextuality is a distinctive feature of quantum theory and a fundamental resource for quantum computation. However, existing examples of contextuality in high-dimensional systems lack the necessary robustness required in experiments. Here we address this problem by identifying a family of noncontextuality inequalities whose maximum quantum violation grows with the dimension of the system. At first glance, this contextuality is the single-system version of multipartite Bell nonlocality taken to an extreme form. What is interesting is that the single-system version achieves the same degree of contextuality but uses a Hilbert space of *lower* dimension. That is, contextuality “concentrates” as the degree of contextuality per dimension increases. We show the practicality of this result by presenting an experimental test of contextuality in a seven-dimensional system. By simulating sequences of quantum ideal measurements with destructive measurements and reparation in an all-optical setup, we report a violation of 68.7 standard deviations of the simplest case of the noncontextuality inequalities identified. Our results advance the investigation of high-dimensional contextuality, its connection to the Clifford algebra, and its role in quantum computation.

Introduction.—In quantum theory, measurements cannot be considered as revealing preexisting properties that are independent of other compatible observables measured on the same system. This phenomenon is called contextuality or Kochen-Specker contextuality [1, 2]. It constitutes a fundamental resource for some quantum information processing tasks [3, 4] and some forms of universal quantum computation such as magic state distillation [5, 6] and measurement-based quantum computation [7–9].

However, a fundamental problem is that arguably the most interesting forms of contextuality are experimentally inaccessible as they require high-dimensional quantum systems unavailable within current experimental platforms (for an extended discussion, see [10]). This problem affects extreme forms of contextuality [11, 12], interesting temporal correlations [13, 14], practical applications of contextuality such as dimension witnessing [15, 16], self-testing [17, 18], sequential measurements-based machine learning [19], and topologically protected quantum computation [20]. To attack this problem, one way is by looking for new high-dimensional systems [10]. Another complementary approach is to identify forms of contextuality that are much more robust to noise.

The objective of this work is to produce robust contextuality in high-dimensional quantum systems. The strategy we follow is looking for extreme forms of Bell nonlocality, which are multipartite versions of contextuality, and using the graph-theoretical approach to quantum correlations [21] to study single-particle versions of them. We observe that we can preserve the degree of contextuality but use a smaller dimensional quantum system. That is, there is a kind of “concentration” of contextuality in the transition between the multipartite and the single-particle cases. As a consequence, sequential measurements on a high-dimensional indivisible system can lead to quantum correlations whose violations of the corresponding noncontextuality inequalities grow with the system dimension. Moreover, the violations require Hilbert spaces smaller than that of the composite system manifesting the same degree of contextuality. This enhances the contextual correlation’s robustness to noise and allows us to experimentally observe contextuality in high-dimensional systems. To demonstrate our findings, we report the experimental results of a path-encoded photonic qudit of $d = 7$ which yields, when quantified by the quantum–classical ratio [12], the highest degree of contextuality ever observed on a single system.

Method.—Bell nonlocality can be seen as a form of contextuality in which the requirement for compatibility is achieved using observables acting on spatially separated subsystems. Therefore, one can trivially convert every violation of a Bell inequality into a violation of a non-contextuality inequality that preserves both the degree of contextuality and the dimension of the Hilbert space [22, 23]. A more intriguing approach is to associate every Bell operator with a graph indicating the exclusivity of a set of Bell experiment events [21], that is, to specify which pairs of events are impossible to happen simultaneously. Then, by identifying a contextuality witness that shares the same graph of exclusivity, we can achieve a greater quantum violation and/or employ smaller dimensional systems [24–27].

Our starting point is the observation that the n -qubit Mermin-Ardehali-Belinskii-Klyshko (MABK) Bell inequalities [28–30] have maximum quantum violations that saturate the no-signaling bound and grow exponentially with the number of qubits. Using the graphs of exclusivity of each Bell MABK operator, we identify a family of noncontextuality inequalities that admit a single-particle realization. We then show that the minimal Hilbert space dimension required to achieve its maximal quantum violation is smaller than that needed to achieve the maximal quantum violation of the corresponding MABK inequalities. This phenomenon, hereafter called “contextuality concentration”, is not limited to the MABK inequalities but also occurs for the bipartite three-settings Bell inequality [26, 31] and, as shown here, for the Bell inequalities for graph states [32–34]. Our emphasis on the MABK inequalities is motivated by their high degree of nonlocality, resistance to noise, and low requirement of critical detection efficiency [35].

Extreme contextuality in high dimensions.—The MABK inequalities for the n -party, two-setting, two-outcome or $(n, 2, 2)$ Bell scenarios with $n \geq 3$ odd can be written as [28]:

$$\mathcal{M}_n = \langle M_n \rangle \stackrel{\text{NCHV}}{\leq} 2^{(n-1)/2}, \quad (1)$$

where $\mathcal{M}_n = \frac{1}{2i} \sum_{\nu \in \{\pm 1\}} \nu \otimes_{j=1}^n (A_1^{(j)} + i\nu A_2^{(j)})$ and the operators $A_k^{(j)}$, $k \in \{0, 1, 2\}$ have eigenvalues ± 1 . The superscripts differentiate the index of qubits, $\langle \cdot \rangle$ indicates expectation value and NCHV means the inequality holds for any noncontextual hidden-variable theory. Its maximal quantum violation, $\mathcal{M}_n = 2^{n-1}$, is achieved by choosing Pauli-like operators $[A_1^{(j)}, A_2^{(j)}] = 2iA_0^{(j)}$ which pairwise anti-commute, and using the GHZ state $|\text{GHZ}_n\rangle = \left(\otimes_{j=1}^n |A_+^{(j)}\rangle + i \otimes_{j=1}^n |A_-^{(j)}\rangle \right) / \sqrt{2}$, with $|A_{\pm}^{(j)}\rangle$ being the ± 1 -eigenstate of $A_0^{(j)}$.

To apply the graph-theoretic approach, we rewrite M_n as a linear combination of rank-1 projectors: $M_n = \sum_{k=1}^{2^{2n-2}} \Pi_k - \sum_{k=1}^{2^{2n-2}} \Pi'_k$. The exponent $2n - 2$ is due

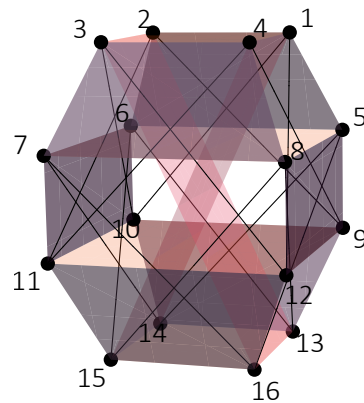


Fig. 1. The graph of exclusivity associated with the events in μ_n for $n = 3$. The points connected by a line represent pairs of mutually exclusive events. The four points on a colored quadrilateral represent four mutually exclusive events.

to that M_n has 2^{n-1} terms and each term has 2^{n-1} positive (negative) projectors. By keeping only the projectors with positive signs, a witness of contextuality can be expressed in terms of event probabilities. Explicitly, $\mu_n = \sum_{k=1}^{2^{2n-2}} \langle \Pi_k \rangle = \mathcal{M}_n/2 + 2^{n-2}$. Let us call G_n the graph of exclusivity of the events in μ_n ; we illustrate the case of $n = 3$ in Fig. 1 and elaborate the procedure in Supplemental Material [36]. According to the graph-theoretic approach, the noncontextual bound and quantum maximum of μ_n are

$$\mu_n \stackrel{\text{NCHV}}{\leq} \alpha(G_n) = 2^{(n-3)/2} + 2^{n-2} \stackrel{\text{Q}}{\leq} \vartheta(G_n) = 2^{n-1}, \quad (2)$$

where $\alpha(G_n)$ and $\vartheta(G_n)$ are the independence and Lovász numbers of G_n , respectively [21]. The first observation is that the gap between noncontextuality and quantum theory is $\vartheta/\alpha = 2 - 2/(1 + 2^{(n-1)/2})$, and thus increases with n .

We now proceed to show that the new graph-theoretic inequality (2) is stronger than the MABK inequality (1), in the sense that the quantum maximum of μ_n exploits only $2^n - 1$ -dimensional Hilbert space—one less than in the n -qubit Bell scenario. The proof is by explicit construction. Let us denote the juxtaposition of the projectors in Eq. (2) as $\mathcal{A} = (\Pi_1 \Pi_2 \cdots \Pi_{2^{2n-2}})$, then,

$$\text{rank}(\mathcal{A}) = 2^n - \dim(\text{solution space of } \mathcal{A}\mathbf{x} = \underbrace{\mathbf{00} \cdots \mathbf{0}}_n), \quad (3)$$

where \mathbf{x} is a 2^n -dimensional ray. However, the only solution to $\mathcal{A}\mathbf{x} = \mathbf{00} \cdots \mathbf{0}$ is a phase-flipped GHZ state: $A_0^{(1)} |\text{GHZ}_n\rangle = \left(\otimes_{j=1}^n |A_+^{(j)}\rangle - i \otimes_{j=1}^n |A_-^{(j)}\rangle \right) / \sqrt{2}$. To check the validity of the solution we observe that, as $A_0^{(1)}$ and $A_1^{(1)}(A_2^{(1)})$ anti-commute, an additional $A_0^{(1)}$ in the state will cause every term in Eq. (1) to inverse sign; Therefore, for the phase-flipped GHZ state, $\mathcal{M}_n =$

-2^{n-1} . Translating it into the event probabilities, we immediately find that μ_n evaluates to 0. The solution is unique because only the GHZ state maximally violates Eq. (1). Consequently, the projectors in \mathcal{A} span only a $2^n - 1$ -dimensional space and can be realized in a quantum system with the same dimension.

The above results show that some forms of multipartite nonlocality can be considered originating from contextuality in lower dimensions and, reciprocally, that some forms of multipartite nonlocality can be “concentrated” into single-particle contextuality with a dimension advantage. In addition, the maximal quantum violation of Eq. (2) can be efficiently obtained by the semidefinite program of Lovász optimization [16]; one possible realization for the $n = 3$ case is given in Supplementary Material [36]. This is in stark contrast with the situation in Bell nonlocality, where the maximal violation is not decidable even with a hierarchy of semidefinite programs [59].

High-dimensional contextuality without inequalities.—Just as nonlocality can be revealed by Hardy- and GHZ-type proofs [60, 61] without using inequalities, the same can be done for contextuality [62–64]. However, no constructions of such proof are known for high-dimensional systems.

Here, we report a large class of logical contextuality from the exclusivity structures of the so-called graph states [65, 66]. Using Clifford algebra, we prove in Supplementary Material [36] that, if the representation of an n -qubit graph state has an odd number of vertices and at least one universal vertex, the events corresponding to the GHZ-type nonlocality produced by the graph state will induce a graph of exclusivity that can be implemented in a $2^n - 1$ -dimensional Hilbert space. Therefore, graph states are ideal candidates for showcasing examples of contextuality concentration. Moreover, our construction here can secure a 100% success probability of observing the Hardy-like events violating noncontextuality, thus paving the way for a robust experimental observation of logical contextuality in high-dimensional systems.

We develop the case $n = 3$, where the graph state, up to local operations, is the GHZ state. In this case, the graph of exclusivity coincides with the one of the $n = 3$ MABK inequality. Subjecting to the graph of exclusivity depicted in Fig. 1, the logical contextuality can be formulated as:

$$\begin{aligned} \sum_{i=1}^4 P(1|i) = 1, \quad \sum_{i=5}^8 P(1|i) = 1, \quad \sum_{i=9}^{12} P(1|i) = 1, \\ \hline \hline 1 \stackrel{\text{Q}}{=} P_{\text{suc}} := \sum_{i=13}^{16} P(1|i) \stackrel{\text{NCHV}}{=} 0. \quad (4) \end{aligned}$$

Here, $P(1|i)$ denotes the probability that the measurement outcome of the observable Π_i is 1 and P_{suc} is the success probability for observing events forbidden in non-contextuality theories. The proof of Eq. (4) and the settings of projectors achieving the quantum maximum are deferred to Supplemental Material [36].

Experiment.—We present an experimental test of the simplest case of the noncontextuality inequalities in (2) with measurements on a seven-dimensional quantum system. The system is encoded in the photonic path degree of freedom and our experiment utilizes the techniques of spatial light modulation [67–69].

The main technical challenge of the experiment is to acquire the statistics of two-point sequential measurements with a photonic seven-dimensional system, which is an open technical problem for dimensions high enough for observing contextuality concentration. To this objective, we have devised a quantum-inspired procedure to realize a non-demolition measurement with destructive measurements followed by a reparation of the post-measurement state [70]. The procedure allowed us to emulate a sequence of two ideal measurements (i.e., yielding the same outcome when repeated and not disturbing compatible observables) of two rank-one projectors Π_i and Π_j with simple prepare-and-measure experiments [71, 72]. Concretely, it works as follows: first, perform a destructive measurement of Π_i . If the measurement yields the outcome 1, then prepare the state $|i\rangle$; if it yields the outcome 0, then prepare $|\psi\rangle - \langle i|\psi\rangle|i\rangle$, that is, the initial state with the $+1$ -eigenstate of Π_i subtracted. Finally, measure Π_j on the reprepared state. Crucially, the context-independent, repeatable, and minimally disturbing nature of the procedure would allow us to justify the assumption of noncontextuality by resorting to classical physics. Therefore, violation of a noncontextuality inequality via the procedure certifies the experiment itself is indeed manifesting contextuality.

To witness the high-dimensional contextuality, we extracted three kinds of quantities from the results of the prepare-and-measure experiment: (i) the probabilities in Eq. (4) demonstrating the Hardy-type contextuality; (ii) the quality of exclusivity, i.e., $\{P(i, j|1, 1) \mid [\Pi_i, \Pi_j] = 0\}$ for establishing a lower bound of μ_3 with realistic measurements and check the measurement repeatability; and (iii) the absence of signaling between compatible measurements for confirming the ideality of the measurement and showing the observed effect was indeed due to contextuality, instead of disturbance. Explicitly, for estimating μ_3 under imperfect exclusivity, we used the fact that [70],

$$\mu_3 \geq \sum_k P(1|k) - \sum_{(i,j)} P(1, 1|i, j), \quad (5)$$

where $k \in V(G_3)$ is an index associated with a vertex in G_3 and $(i, j) \in E(G_3)$ is an edge in G_3 . The no-signaling condition between pairs of compatible observables Π_i and Π_j can be verified by checking if all the following signaling factors vanish:

$$\begin{aligned} \varepsilon_{ij} &= P(1|i) - P(1, _ |i, j), & \varepsilon'_{ij} &= P(1|i) - P(_, 1 |j, i), \\ \varepsilon_{ji} &= P(1|j) - P(1, _ |j, i), & \varepsilon'_{ji} &= P(1|j) - P(_, 1 |i, j). \end{aligned} \quad (6)$$

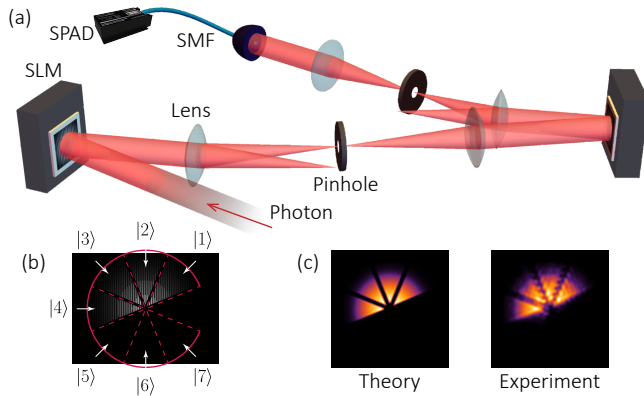


Fig. 2. Experimental setup. (a) Optical setup of the prepare-and-measure experiment. A spatial light modulator (SLM) encoded the initial state by modulating the photonic wavefront. A $4f$ -correlator mapped the wavefront to the second SLM which implemented the measurement. The photons are collected by a single-mode fiber (SMF) and sent to the single-photon avalanche detector (SPAD) for photon counting. (b) A sample hologram showing the encoding scheme. The corresponding state is $|\psi\rangle = (|1\rangle + |2\rangle + |3\rangle + |4\rangle)/2$. (c) An example of calculated versus measured wavefunction profile. The holograms and their characterization results for all states (projectors) needed in the experiment are shown in Supplemental Material [36].

That is, the marginal probability of one measurement is statistically independent of the other, regardless of the sequence of two measurements performed. Here, $P(1, _ | i, j) = P(1 | j)P(1 | i = 1, j) + P(0 | j)P(1 | i = 0, j)$ denotes the marginal probability of Π_i yielding outcome 1 when Π_j is subsequently measured; similarly definitions hold for the other marginal probabilities.

Our experimental setup is illustrated in Fig. 2(a). Photons from an attenuated 800 nm laser were expanded and the wavefront resembled a Gaussian beam with a waist radius of 1.6 mm. Throughout the experiment, we used the spatial mode degree of freedom of the photons to register the seven-dimensional qudit, where the computational bases $|1\rangle$ through $|7\rangle$ are the angular states localized within a circular sector of the Gaussian beam. To generate these angular states and their superpositions, we casted photons on a spatial light modulator (SLM) that displayed a phase-only hologram of seven circular sectors (cf. Fig. 2(b)). The hologram in each sector displayed a blazed grating with a different phase range; consequently, a fraction of photons underwent diffraction, resulting in their propagation direction being altered towards the second SLM. By adjusting the maximum phase variation of the grating to control the amplitude of photon wavefunctions in the seven sectors, we can realize the encoding of arbitrary qudit states [73], with an explicit example shown in Fig. 2(c).

The modulated photons then propagated through a $4f$ -correlator, where the unwanted diffraction orders were fil-

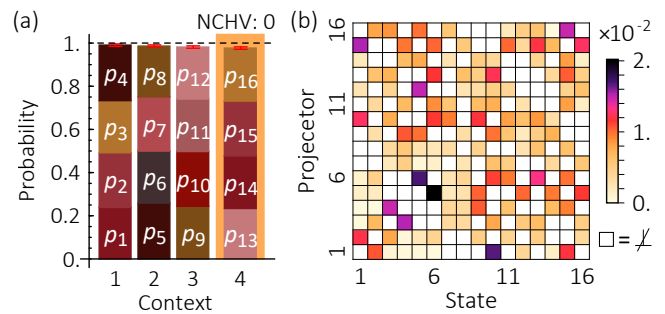


Fig. 3. Experimental results. (a) Stacked bar chart of event probabilities with the 7-dimensional photonic system. Given all prerequisites in former columns. The last column with orange background has noncontextual (quantum) predictions of ideally 0(1), therefore manifesting logical contextuality. The error bars denote the 1σ standard deviations calculated by assuming a Poissonian counting statistics. (b) Orthogonality between the projectors measured determined by preparing the nondegenerate eigenstate of every projector and measuring the detection probabilities on their corresponding compatible projectors. Only the grids corresponding to different compatible measurements are colored (the others are white).

tered by a pinhole at the focal plane of the first lens. At the output plane of the correlator, a second SLM implemented the qudit measurement by employing the reverse transformation of the encoding process [75, 76]. In this way, choices of the initial states and the measurement settings were realized by displaying different holograms on the first and second SLM, respectively. To check the precision of the setup, we prepared all holograms used in the experiment, measured the spatial wavefunction profiles directly before the second SLM with a charge-coupled device camera, and compared them with theoretical predictions (cf. Supplemental Material [36]). The results revealed an average Pearson correlation [74] of 95.5% between theoretical and experimental wavefunction profiles. Finally, a telescope shrank the beam waist, and the photons were collected by a single-mode fiber (SMF) to determine the detection probability of an initial state on a specific measurement basis with photon counting.

Our experimental results are presented in Fig. 3. For the observation of Hardy-like contextuality (4), we displayed the hologram of the initial state on the first SLM and iterated the holograms on the second SLM over all the measurement basis. The total probabilities on the left-hand sides of the three constraints and the final non-classical event were measured to exceed 97.6%, exhibiting a sharp contradiction with the prediction from non-contextuality. To ensure reasonable exclusivity of the compatible measurements in the experiment, pairs of holograms corresponding to orthogonal projectors were displayed on the two SLMs. The average detection probabilities for these settings were determined to be $P(1, 1 | i, j) = 0.64\%$ —almost vanishing as expected for ideal measurements. By substituting the recorded proba-

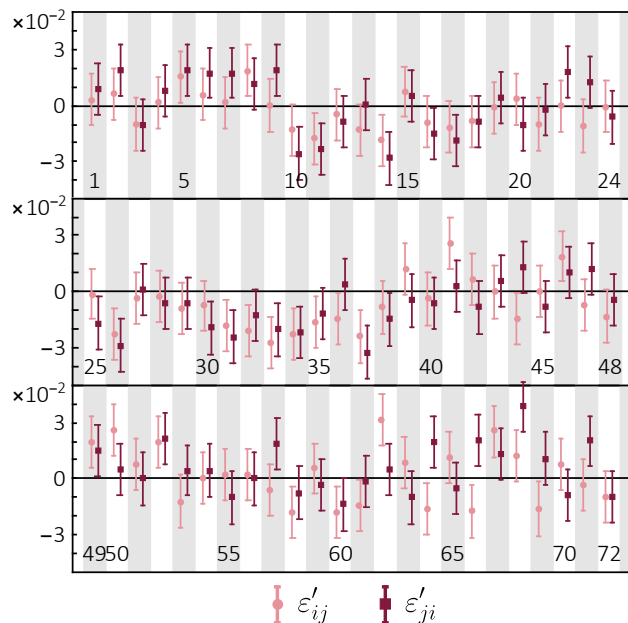


Fig. 4. Verification of no-signaling condition. The numbers stand for indices of edges $(i, j) \in G_3$, sorted by i then j with $i < j$. The data points denote signaling factors and the error bars denote the 1σ standard deviations calculated by assuming a Poissonian counting statistics.

bilities into Eq. (5) to compensate for the deviations from ideal exclusivity and test the quantitative noncontextuality inequality, we found that $\mu_3 \geq 3.821 \pm 0.012$, violating the prediction of noncontextuality by 68.7 standard deviations. Here, the standard deviations were estimated by assuming a Poisson distribution for the statistics and resampling the recorded data (cf. Supplemental Material [36]).

To verify the no-signaling condition, we prepared the conditional state after the first projector measurement for each edge in the exclusivity graph G_3 , and then measured it with the second projector. Owing to the normalization of counting, the effect of a later measurement upon an earlier one, represented by ε_{ij} and ε_{ji} , would always be zero. The result of ε'_{ij} and ε'_{ji} in the no-signaling test for the 72 edges in G_3 is shown in Fig. 4. Most of the signaling factors are within one standard deviation from zero, with a quantitative characterization gave $|\overline{\varepsilon'}| = (1.17 \pm 1.39)\%$. The small nonzero values can be considered to originate from experimental imprecision and small drifting over time, and the overall results complied well with the no-signaling requirement.

Conclusions.—We have identified quantum correlations resulting from sequential measurements on a single particle that manifest extremely strong forms of contextuality in lower dimensions. These correlations exhibit large violations of noncontextuality inequalities and perfect success probabilities for single-shot detection of contextuality. An accompanying photonic experiment

fleshed out the theoretical findings by simulating sequences of ideal quantum measurements with destructive measurements and observed the highest degree of contextuality on a single system (cf. Supplemental Material [36] for a comparison with previous studies). Although the present result only shows a dimension reduction of 1, we envisage that contextuality concentration can be scalable by utilizing graph products, thereby offering additional advantages. Because contextuality in stabilizer subtheory-based exclusivity structures investigated here forms the backbone of quantum computation architectures [5–9, 77–79] in many different physical systems [20, 80–91], our work may stimulate the development of high-dimensional quantum information processing and novel quantum algorithms.

We would like to thank Yu Meng and Ze-Yan Hao for insightful comments and Shihao Ru, Carles Roch i Carceller, and Abhinav Verma for helpful feedback on an earlier version of the paper. This work was supported by the Innovation Program for Quantum Science and Technology (Grant No. 2021ZD0301400), the National Natural Science Foundation of China (Grants Nos. 61725504, 11821404, and U19A2075), the Fundamental Research Funds for the Central Universities (Grant No. WK2030000056), and the Anhui Initiative in Quantum Information Technologies (Grant No. AHY060300). J.L.C. was supported by the National Natural Science Foundations of China (Grant Nos. 12275136, 11875167 and 12075001), the 111 Project of B23045, and the Fundamental Research Funds for the Central Universities (Grant No. 3072022TS2503). H.X.M. was supported by the National Natural Science Foundations of China (Grant No. 11901317). Z.P.X. was supported by the Alexander Humboldt foundation. A.C. is supported by the MCIN/AEI Project No. PID2020-113738GB-I00, Project Qdisc (Project No. US-15097, Universidad de Sevilla), with FEDER funds, and QuantERA grant SECRET (MCIN/AEI Project No. PCI2019-111885-2). This work was partially carried out at the USTC Center for Micro and Nanoscale Research and Fabrication. Z.H.L. and H.X.M. contributed equally to this work.

-
- [1] S. Kochen and E. P. Specker, The Problem of Hidden Variables in Quantum Mechanics, *J. Math. Mech.* **17**, 59 (1967).
 - [2] C. Budroni, A. Cabello, O. Gühne, M. Kleinmann, and J.-Å. Larsson, Quantum Contextuality, *arXiv: 2102.13036*.
 - [3] A. Cabello, V. D’Ambrosio, E. Nagali, and F. Sciarrino, Hybrid ququart-encoded quantum cryptography protected by Kochen-Specker contextuality, *Phys. Rev. A* **84**, 030302(R) (2011).
 - [4] E. Amselem, L. E. Danielsen, A. J. López-Tarrida, J. R. Portillo, M. Bourennane, and A. Cabello, Experimental Fully Contextual Correlations, *Phys. Rev. Lett.*

- 108**, 200405 (2012).
- [5] S. Bravyi and A. Kitaev, Universal quantum computation with ideal Clifford gates and noisy ancillas, *Phys. Rev. A* **71**, 022316 (2005).
 - [6] M. Howard, J. Wallman, V. Veitch, and J. Emerson, Contextuality supplies the ‘magic’ for quantum computation, *Nature* **510**, 351 (2016).
 - [7] R. Raussendorf, Contextuality in measurement-based quantum computation, *Phys. Rev. A* **88**, 022322 (2013).
 - [8] S. Abramsky, R. S. Barbosa, and S. Mansfield, Contextual Fraction as a Measure of Contextuality, *Phys. Rev. Lett.* **119**, 050504 (2017).
 - [9] M. Frembs, S. Roberts, and S. D. Bartlett, Contextuality as a resource for measurement-based quantum computation beyond qubits, *New. J. Phys.* **20**, 103011 (2018).
 - [10] A. Asadian and A. Cabello, Bosonic indistinguishability-dependent contextuality, *Phys. Rev. A* **105**, 012404 (2022).
 - [11] A. Cabello, Proposed test of macroscopic quantum contextuality, *Phys. Rev. A* **82**, 032110 (2010).
 - [12] B. Amaral, M. Terra Cunha, and A. Cabello, Quantum theory allows for absolute maximal contextuality, *Phys. Rev. A* **92**, 062125 (2015).
 - [13] C. Budroni, T. Moroder, M. Kleinmann, and O. Gühne, Bounding Temporal Quantum Correlations, *Phys. Rev. Lett.* **111**, 020403 (2013).
 - [14] C. Budroni and C. Emary, Temporal Quantum Correlations and Leggett-Garg Inequalities in Multilevel Systems, *Phys. Rev. Lett.* **113**, 050401 (2014).
 - [15] O. Gühne, C. Budroni, A. Cabello, M. Kleinmann, and J.-Å. Larsson, Bounding the quantum dimension with contextuality, *Phys. Rev. A* **89**, 062107 (2014).
 - [16] M. Ray, N. G. Boddu, K. Bharti, L.-C. Kwek, and A. Cabello, Graph-theoretic approach to dimension witnessing, *New J. Phys.* **23**, 033006 (2021).
 - [17] K. Bharti, M. Ray, A. Varvitsiotis, N. A. Warsi, A. Cabello, and L.-C. Kwek, Robust Self-Testing of Quantum Systems via Noncontextuality Inequalities, *Phys. Rev. Lett.* **122**, 250403 (2019).
 - [18] K. Bharti, M. Ray, A. Varvitsiotis, A. Cabello, and L.-C. Kwek, Local certification of programmable quantum devices of arbitrary high dimensionality, preprint at [arXiv: 1911.09448](https://arxiv.org/abs/1911.09448).
 - [19] X. Gao, E. R. Anschuetz, S.-T. Wang, I. J. Cirac, and M. D. Lukin, Enhancing Generative Models via Quantum Correlations, preprint at [arXiv: 2101.08354](https://arxiv.org/abs/2101.08354).
 - [20] Z.-H. Liu, K. Sun, J. K. Pachos, M. Yang, Y. Meng, Y.-W. Liao, et al., Topological contextuality and anyonic statistics of photonic-encoded parafermions, *PRX Quantum* **2**, 030323 (2021).
 - [21] A. Cabello, S. Severini, and A. Winter, Graph-Theoretic Approach to Quantum Correlations, *Phys. Rev. Lett.* **112**, 040401 (2014).
 - [22] O. Gühne, M. Kleinmann, A. Cabello, J.-Å. Larsson, G. Kirchmair, F. Zähringer, R. Gerritsma, and C. F. Roos, Compatibility and noncontextuality for sequential measurements, *Phys. Rev. A* **81**, 022121 (2010).
 - [23] A. Cabello, Bell non-locality and Kochen-Specker contextuality: How are they connected?, *Found. Phys.* **51**, 61 (2021).
 - [24] M. Sadiq, P. Badziąg, M. Bourennane, and A. Cabello, Bell inequalities for the simplest exclusivity graph, *Phys. Rev. A* **87**, 012128 (2013).
 - [25] R. Rabelo, C. Duarte, A. J. López-Tarrida, M. Terra Cunha, and A. Cabello, Multigraph approach to quantum non-locality, *J. Phys. A: Math. Theor.* **47**, 424021 (2014).
 - [26] Z.-H. Liu, H.-X. Meng, Z.-P. Xu, J. Zhou, S. Ye, Q. Li, K. Sun, H.-Y. Su, A. Cabello, J.-L. Chen, J.-S. Xu, C.-F. Li, and G.-C. Guo, Experimental observation of quantum contextuality beyond Bell nonlocality, *Phys. Rev. A* **100**, 042118 (2019).
 - [27] M. Ray, N. G. Boddu, K. Bharti, L.-C. Kwek, and A. Cabello, Graph-theoretic approach to dimension witnessing, *New J. Phys.* **23**, 033006 (2021).
 - [28] N. D. Mermin, Extreme quantum entanglement in a superposition of macroscopically distinct states, *Phys. Rev. Lett.* **65**, 1838 (1990).
 - [29] M. Ardehali, Bell inequalities with a magnitude of violation that grows exponentially with the number of particles, *Phys. Rev. A* **46**, 5375 (1992).
 - [30] A. V. Belinskii and D. N. Klyshko, Interference of light and Bell’s theorem, *Phys. Usp.* **36**, 653 (1993).
 - [31] D. Collins and N. Gisin, A relevant two qubit Bell inequality inequivalent to the CHSH inequality, *J. Phys. A: Math. Gen.* **37**, 1775 (2004).
 - [32] O. Gühne, G. Tóth, P. Hyllus, and H. J. Briegel, Bell Inequalities for Graph States, *Phys. Rev. Lett.* **95**, 120405 (2005).
 - [33] O. Gühne and A. Cabello, Generalized Ardehali-Bell inequalities for graph states, *Phys. Rev. A* **77**, 032108 (2008).
 - [34] A. Cabello, O. Gühne, and D. Rodríguez, Mermin inequalities for perfect correlations, *Phys. Rev. A* **77**, 062106 (2008).
 - [35] A. Cabello, D. Rodríguez, and I. Villanueva, Necessary and Sufficient Detection Efficiency for the Mermin Inequalities, *Phys. Rev. Lett.* **101**, 120402 (2008).
 - [36] See Supplemental Material at [Link to Supplemental Material](#) for proofs of the propositions in the main text and experimental details.
 - [37] S.-H. Jiang, Z.-P. Xu, H.-Y. Su, A. K. Pati, and J.-L. Chen, Generalized Hardy’s Paradox, *Phys. Rev. Lett.* **120**, 050403 (2018).
 - [38] Y.-H. Luo, H.-Y. Su, H.-L. Huang, X.-L. Wang, T. Yang, L. Li, N.-L. Liu, J.-L. Chen, C.-Y. Lu, and J.-W. Pan, Experimental test of generalized Hardy’s paradox, *Sci. Bull.* **63**, 1611 (2018).
 - [39] M. Yang, H.-X. Meng, J. Zhou, Z.-P. Xu, Y. Xiao, K. Sun, J.-L. Chen, J.-S. Xu, C.-F. Li, and G.-C. Guo, Stronger Hardy-type paradox based on the Bell inequality and its experimental test, *Phys. Rev. A* **99**, 032103 (2019).
 - [40] N. D. Mermin, Quantum mysteries refined, *Am. J. Phys.* **62**, 880 (1994).
 - [41] A. A. Klyachko, M. A. Can, S. Binicioğlu and A. S. Shumovsky, Simple Test for Hidden Variables in Spin-1 Systems, *Phys. Rev. Lett.* **101**, 020403 (2008).
 - [42] R. Lapkiewicz, P. Li, C. Schaeff, N. K. Langford, S. Ramelow, M. Wieśniak, and A. Zeilinger, Experimental non-classicality of an indivisible quantum system, *Nature* **474**, 490 (2011).
 - [43] E. Amsalem, M. Rådmark, M. Bourennane, and A. Cabello, State-independent quantum contextuality with single photons, *Phys. Rev. Lett.* **103**, 160405 (2009).
 - [44] O. Moussa, C. A. Ryan, D. G. Cory, and R. Laflamme, Testing contextuality on quantum ensembles with one clean qubit, *Phys. Rev. Lett.* **104**, 160501 (2010).

- [45] E. Nagali, V. D'Ambrosio, F. Sciarrino, and A. Cabello, Experimental observation of impossible-to-beat quantum advantage on a hybrid photonic system, *Phys. Rev. Lett.* **108**, 090501 (2012).
- [46] J. Ahrens, E. Amsellem, A. Cabello, and M. Bourennane Two fundamental experimental tests of nonclassicality with qutrits, *Sci. Rep.* **3**, 2170 (2013).
- [47] Y.-F. Huang, M. Li, D.-Y. Cao, C. Zhang, Y.-S. Zhang, B.-H. Liu, C.-F. Li, and G.-C. Guo, Experimental test of state-independent quantum contextuality of an indivisible quantum system, *Phys. Rev. A* **87**, 052133 (2013).
- [48] X. Zhang, M. Um, J. Zhang, S. An, Y. Wang, D.-L. Deng, C. Shen, L.-M. Duan, and K. Kim, State-independent experimental test of quantum contextuality with a single trapped ion, *Phys. Rev. Lett.* **110**, 070401 (2013).
- [49] G. Cañas, S. Etcheverry, E. S. Gómez, C. Saavedra, G. B. Xavier, G. Lima, and A. Cabello, Experimental implementation of an eight-dimensional Kochen-Specker set and observation of its connection with the Greenberger-Horne-Zeilinger theorem, *Phys. Rev. A* **90**, 012119 (2014).
- [50] G. Cañas, M. Arias, S. Etcheverry, E. S. Gómez, A. Cabello, G. B. Xavier, and G. Lima, Applying the simplest Kochen-Specker set for quantum information processing, *Phys. Rev. Lett.* **113**, 090404 (2014).
- [51] M. Arias, G. Cañas, E. S. Gómez, J. F. Barra, G. B. Xavier, G. Lima, V. D'Ambrosio, F. Baccari, F. Sciarrino, and A. Cabello, Testing noncontextuality inequalities that are building blocks of quantum correlations, *Phys. Rev. A* **92**, 032126 (2015).
- [52] M. Jerger, et al., Contextuality without nonlocality in a superconducting quantum system, *Nat Commun* **7**, 12930 (2016).
- [53] A. Crespi, M. Bentivegna, I. Pitsios, D. Rusca, D. Poderini, G. Carvacho, V. D'Ambrosio, A. Cabello, F. Sciarrino, and Roberto Osellame, Single-photon quantum contextuality on a chip, *ACS Photonics* **4**, 2807–2812 (2017).
- [54] Y. Xiao, Z.-P. Xu, Q. Li, H.-Y. Su, K. Sun, A. Cabello, J.-S. Xu, J.-L. Chen, C.-F. Li, and G.-C. Guo, Experimental test of quantum correlations from Platonic graphs, *Optica* **5**, 718–722 (2018).
- [55] W.-R. Qi, J. Zhou, L.-J. Kong, Z.-P. Xu, H.-X. Meng, R. Liu, Z.-X. Wang, C. Tu, Y. Li, A. Cabello, J.-L. Chen, and H.-T. Wang, Stronger Hardy-like proof of quantum contextuality, *Photon. Res.* **10**, 1582–1593 (2022).
- [56] S. Ru, W. Tang, Y. Wang, F. Wang, P. Zhang, and F. Li, Verification of Kochen-Specker-type quantum contextuality with a single photon, *Phys. Rev. A* **105**, 012428 (2022).
- [57] D. Qu, K. Wang, L. Xiao, X. Zhan, and P. Xue, State-independent test of quantum contextuality with either single photons or coherent light, *npj Quant. Inf.* **7**, 154 (2021).
- [58] K. Bharti, M. Ray, Z.-P. Xu, M. Hayashi, L.-C. Kwak, and A. Cabello, Graph-theoretic approach for self-testing in Bell scenarios, *PRX Quantum* **3**, 030344 (2022).
- [59] M. Navascués, Y. Guryanova, M. J. Hoban, and Antonio Acín, Almost quantum correlations, *Nat. Commun.* **6**, 6288 (2015).
- [60] L. Hardy, Nonlocality for Two Particles without Inequalities for Almost All Entangled States, *Phys. Rev. Lett.* **71**, 1665 (1993).
- [61] D. M. Greenberger, M. A. Horne, and A. Zeilinger, in *Bell's Theorem, Quantum Theory, and Conceptions of the Universe*, edited by M. Kafatos (Kluwer, Dordrecht, 1989), p. 69.
- [62] A. Cabello, P. Badziag, M. T. Cunha, and M. Bourennane, Simple Hardy-Like Proof of Quantum Contextuality, *Phys. Rev. Lett.* **111**, 180404 (2013).
- [63] B. Marques, J. Ahrens, M. Nawareg, A. Cabello, and M. Bourennane, Experimental Observation of Hardy-Like Quantum Contextuality, *Phys. Rev. Lett.* **113**, 250403 (2014).
- [64] Z.-P. Xu, J.-L. Chen, and O. Gühne, Proof of the Peres Conjecture for Contextuality, *Phys. Rev. Lett.* **124**, 230401 (2020).
- [65] Graph states are a family of highly entangled multiqubit states represented by undirected graphs, not to be confused with the graph of exclusivity in the graph-theoretic approach of contextuality.
- [66] M. Hein, J. Eisert, and H. J. Briegel, Multiparty entanglement in graph states, *Phys. Rev. A* **69**, 062311 (2004).
- [67] E. A. Aguilar, M. Farkas, D. Martínez, M. Alvarado, J. Cariñe, G. B. Xavier, J. F. Barra, G. Cañas, M. Pawłowski, and G. Lima, Certifying an Irreducible 1024-Dimensional Photonic State Using Refined Dimension Witnesses, *Phys. Rev. Lett.* **120**, 230503 (2018).
- [68] X.-M.-Hu, W.-B. Xing, B.-H. Liu, Y.-F. Huang, C.-F. Li, G.-C. Guo, P. Erker, and M. Huber, Efficient Generation of High-Dimensional Entanglement through Multipath Down-Conversion, *Phys. Rev. Lett.* **125**, 090503 (2020).
- [69] D. Pierangeli, G. Marcucci, and C. Conti, Large-Scale Photonic Ising Machine by Spatial Light Modulation, *Phys. Rev. Lett.* **122**, 213902 (2019).
- [70] A. Cabello, Simple method for experimentally testing any form of quantum contextuality, *Phys. Rev. A* **93**, 032102 (2016).
- [71] G. Cañas, E. Acuña, J. Cariñe, J. F. Barra, E. S. Gómez, G. B. Xavier, G. Lima, and A. Cabello Experimental demonstration of the connection between quantum contextuality and graph theory, *Phys. Rev. A* **94**, 012337 (2016).
- [72] Y. Xiao, Z.-P. Xu, Q. Li, J.-S. Xu, K. Sun, J.-M. Cui, Z.-Q. Zhou, H.-Y. Su, A. Cabello, J.-L. Chen, C.-F. Li, and G.-C. Guo. Experimental observation of quantum state-independent contextuality under no-signaling conditions, *Opt. Express* **26**, 32 (2018).
- [73] E. Bolduc, N. Bent, E. Santamato, E. Karimi, and R. W. Boyd, Exact solution to simultaneous intensity and phase encryption with a single phase-only hologram, *Opt. Lett.* **38**, 3546 (2013).
- [74] J. L. Rodgers and W. A. Nicewander, Thirteen ways to look at the correlation coefficient, *Am. Stat.* **42**, 59 (1988).
- [75] V. D'Ambrosio, F. Cardano, E. Karimi, E. Nagali, E. Santamato, L. Marrucci, and F. Sciarrino, Test of mutually unbiased bases for six-dimensional photonic quantum systems, *Sci. Rep.* **3**, 2726 (2013).
- [76] N. Bent, H. Qassim, A. A. Tahir, D. Sych, G. Leuchs, L. L. Sánchez-Soto, E. Karimi, and R. W. Boyd, Experimental Realization of Quantum Tomography of Photonic Qudits via Symmetric Informationally Complete Positive Operator-Valued Measures, *Phys. Rev. X* **5**, 041006 (2015).
- [77] N. Delfosse, P. A. Guerin, J. Bian, and R. Raussendorf, Wigner Function Negativity and Contextuality in Quantum Computation on Rebits, *Phys. Rev. X* **5**, 021003 (2015).

- (2015).
- [78] F. Shahandeh, Quantum computational advantage implies contextuality, preprint at [arXiv: 2112.00024](https://arxiv.org/abs/2112.00024).
- [79] R. I. Booth, U. Chabaud, and P. -E. Emeriau, Contextuality and Wigner negativity are equivalent for continuous-variable quantum measurements, preprint at [arXiv: 2111.13218](https://arxiv.org/abs/2111.13218).
- [80] A. M. Souza, J. Zhang, C. A. Ryan, and R. Laflamme, Experimental magic state distillation for fault-tolerant quantum computing, *Nat. Commun.* **2**, 169 (2011).
- [81] M. Mamaev, R. Blatt, J. Ye, and A. M. Rey, Cluster State Generation with Spin-Orbit Coupled Fermionic Atoms in Optical Lattices, *Phys. Rev. Lett.* **122**, 160402 (2019).
- [82] L. Egan, D. M. Debroy, C. Noel, A. Risinger, D. Zhu, D. Biswas, M. Newman, M. Li, K. R. Brown, M. Cetina, and C. Monroe, Fault-tolerant control of an error-corrected qubit, *Nature* **598**, 281 (2021).
- [83] H.-L. Huang *et al.*, Emulating Quantum Teleportation of a Majorana Zero Mode Qubit, *Phys. Rev. Lett.* **126**, 090502 (2021).
- [84] G. Waldherr, Y. Wang, S. Zaiser, M. Jamali, T. Schulte-Herbrüggen, H. Abe, T. Ohshima, J. Isoya, J. F. Du, P. Neumann, and J. Wrachtrup, Quantum error correction in a solid-state hybrid spin register, *Nature* **506**, 204 (2014).
- [85] C. P. Michaels, J. A. Martínez, R. Debroux, R. A. Parker, A. M. Stramma, L. I. Huber, C. M. Purser, M. Atatüre, and D. A. Gangloff, Multidimensional cluster states using a single spin-photon interface coupled strongly to an intrinsic nuclear register, *Quantum* **5**, 565 (2021).
- [86] A. Bourassa, C. P. Anderson, K. C. Miao, M. Onizhuk, H. Ma, A. L. Crook, H. Abe, J. Ul-Hassan, T. Ohshima, N. T. Son, G. Galli, and D. D. Awschalom, Entanglement and control of single nuclear spins in isotopically engineered silicon carbide, *Nat. Mater.* **19**, 1319 (2020).
- [87] M. H. Abobeih, Y. Wang, J. Randall, S. J. H. Loenen, C. E. Bradley, M. Markham, D. J. Twitchen, B. M. Terhal, and T. H. Taminiau, Fault-tolerant operation of a logical qubit in a diamond quantum processor, *Nature* **606**, 884 (2022).
- [88] J. Eli Bourassa *et al.*, Blueprint for a Scalable Photonic Fault-Tolerant Quantum Computer, *Quantum* **5**, 392 (2021).
- [89] M. V. Larsen, X. Guo, C. R. Breum, J. S. Neergaard-Nielsen, and U. L. Andersen, Deterministic generation of a two-dimensional cluster state, *Science* **366**, 369 (2019).
- [90] W. Asavanant, Y. Shiozawa, S. Yokoyama, B. Charoensombutamon, H. Emura, R. N. Alexander, S. Takeda, J. Yoshikawa, N. C. Menicucci, H. Yonezawa, and A. Furusawa, Generation of time-domain-multiplexed two-dimensional cluster state, *Science* **366**, 373 (2019).
- [91] M. V. Larsen, X. Guo, C. R. Breum, J. S. Neergaard-Nielsen, and U. L. Andersen, Deterministic multi-mode gates on a scalable photonic quantum computing platform, *Nat. Phys.* **17**, 1018 (2021).

Supplementary Material for “Experimental Test of High-Dimensional Quantum Contextuality Based on Contextuality Concentration”

In this Supplemental Material, we start by summarizing the graph-theoretical approach to contextuality, and use it to derive the simplest case of contextuality concentration from the tripartite Mermin–Ardehali–Belinskii–Klyshko (MABK) inequality to a noncontextuality inequality whose maximal quantum violation can be saturated using a set of 7-dimensional state and projectors. We then prove a construction of logical contextuality from a family of Greenberger–Horne–Zeilinger- (GHZ)-type paradoxes in graph states [1] and show the resulted logical contextuality can be achieved in a Hilbert space whose dimension is less than the graph state. After that, we showcase the simplest case among the above logical contextuality using its graph of exclusivity and give a set of 7-dimensional rays manifesting the logical contextuality with a success probability of 100%. This setting also maximally violates the simplest case of the family of noncontextual hidden-variable (NCHV) inequalities in the main text and is used in our experimental test. Further, we present more details about the experiment and data analysis. Finally, we conclude with a summary of results in single-particle-based contextuality tests to show the merit of contextuality concentration for generating a high degree of contextuality.

CONTENTS

A. A brief summary of the graph-theoretic approach to contextuality	1
B. From the MABK inequality to the graph of exclusivity	2
C. Logical contextuality from the graph states	4
D. Direct proof of the logical contextuality (3) in the main text	5
E. Experimental details	6
F. Data analysis	7
G. Summary of results: single-particle tests of contextuality	11
References	13

Appendix A: A brief summary of the graph-theoretic approach to contextuality

A modern method of bounding the set of behaviors of quantum correlation is the graph-theoretic approach [2]. We say a behavior is a set of probability distributions derived from projective measurements over arbitrary quantum states. Due to the orthogonality of measurements, some events cannot happen simultaneously. The graph of exclusivity G essentially captures this impossibility: its vertices $V(G)$ represent the events of observing certain measurement outcomes, and its edges $E(G)$ connect pairs of exclusive events. The graph-theoretic approach treats correlations of general observables by expressing them in terms of linear combination of probabilities of events.

Once a graph of exclusivity is given, the set of noncontextual and quantum correlations it can support is determined by the stable set polytope $\text{STAB}(G)$ and theta body $\text{TH}(G)$, respectively:

$$\begin{aligned} \text{STAB}(G) &:= \text{conv} \left\{ x \in \{0, 1\}^{|V|} \mid x_i x_j = 0, \forall (i, j) \in E \right\}, \\ \text{TH}(G) &:= \left\{ p \in \mathbb{R}_+^{|V|} \mid p_i = |\langle \psi | v_i \rangle|^2, \{ |v\rangle\} \text{ OR of } \bar{G} \right\}, \end{aligned} \quad (\text{S1})$$

where \bar{G} is graph complement of G , conv and OR denote convex combination and orthogonal representation. The sum of event probabilities in NCHV and quantum theories are thus bounded by graph constants, namely, the independence number and Lovász number [3]:

$$\sum_{i \in V(G)} P(1|i) - \sum_{(i,j) \in E(G)} P(1, 1|i, j) \stackrel{\text{NCHV}}{\leq} \alpha(G) \stackrel{\text{Q}}{\leq} \vartheta(G). \quad (\text{S2})$$

Here, $P(1, 1|i, j)$ is the probability of observing (ideally) exclusive events i, j simultaneously happen in one experiment; this term compensates for the deviation from exclusivity. Graphs with a large ϑ/α ratio has the merit of producing significant inconsistency between noncontextuality and quantum theories.

Appendix B: From the MABK inequality to the graph of exclusivity

The derivation in the main text, section “*Extreme contextuality in high dimensions*” is based on the device-independent form of MABK inequality for better generality. However, contextuality concentration exists in more general scenarios and does not depend on knowledge about MABK inequality to be interpreted. In this section, we will reiterate the derivation in a pedagogical manner and using explicit Pauli operators. We hope that, by coming through the derivation here, even readers not familiar with multipartite Bell nonlocality and the graph-theoretical approach of contextuality should be able to follow the result and gain insight into contextuality concentration. In order to improve the readability, throughout this Supplemental Material, we will use the shorthand notation $\{X, Y, Z\} \equiv \{\sigma_x, \sigma_y, \sigma_z\} = \left\{ \begin{pmatrix} 0 & 1 \\ 1 & 0 \end{pmatrix}, \begin{pmatrix} 0 & -i \\ i & 0 \end{pmatrix}, \begin{pmatrix} 1 & 0 \\ 0 & -1 \end{pmatrix} \right\}$ to represent the Pauli operators, and $\{\Pi_{\pm x}, \Pi_{\pm y}, \Pi_{\pm z}\} \equiv \left\{ \frac{\mathbb{I} + X}{2}, \frac{\mathbb{I} + Y}{2}, \frac{\mathbb{I} + Z}{2} \right\}$ to denote the projectors corresponding to their ± 1 -eigenstate.

To keep the discussion self-contained, we rewrite the definition of the MABK inequality, which is the same as the Eq. (1) in the main text. For $n \geq 3$ odd:

$$M_n = \frac{1}{2i} \left[\bigotimes_{j=1}^n (A_1^{(j)} + iA_2^{(j)}) - \bigotimes_{j=1}^n (A_1^{(j)} - iA_2^{(j)}) \right], \quad \mathcal{M}_n = \langle M_n \rangle \stackrel{\text{NCHV}}{\leq} 2^{(n-1)/2}. \quad (\text{S1})$$

By explicit expansion, M_n can also be expanded as:

$$M_n = \sum_{k=0}^{(n-1)/2} (-1)^k \pi \left(\bigotimes_{j=1}^{2k+1} A_2^{(j)} \bigotimes_{j=2k+2}^n A_1^{(j)} \right), \quad (\text{S2})$$

where the symbol π means the summation of permutations of the superscripts that give distinct products. The total number of terms in M_n then can be calculated to be $\sum_{k=0}^{(n-1)/2} \binom{n}{2k+1} = 2^{n-1}$.

We now focus only on the simplest (3-qubit) case of the family of inequalities and use the Pauli operators to replace the abstract operators $A_k^{(j)}$, $k \in \{0, 1, 2\}$. Although the choices of these operators are arbitrary, following Mermin’s convention, we shall use $A_1^{(j)} = X^{(j)}$, $A_2^{(j)} = Y^{(j)}$, and $A_0^{(j)} = Z^{(j)}$ so the maximal quantum violation is achievable using the GHZ-state. Substituting the above convention into Eq. (S2), we have:

$$\begin{aligned} M_3 &= \pi \left(Y^{(1)} X^{(2)} X^{(3)} \right) - \pi \left(Y^{(1)} Y^{(2)} Y^{(3)} \right) \\ &= Y^{(1)} X^{(2)} X^{(3)} + X^{(1)} Y^{(2)} X^{(3)} + X^{(1)} X^{(2)} Y^{(3)} - Y^{(1)} Y^{(2)} Y^{(3)}, \quad \mathcal{M}_3 = \langle M_3 \rangle \stackrel{\text{NCHV}}{\leq} 2. \end{aligned} \quad (\text{S3})$$

We can also check that the 3-qubit GHZ-state is $|\text{GHZ}_3\rangle = (|000\rangle + i|111\rangle)/\sqrt{2}$, and $\langle \text{GHZ}_3 | M_3 | \text{GHZ}_3 \rangle = 4$.

To recast the MABK operator into event-probability form, we use the projector expansion $X = \Pi_{+x} - \Pi_{-x}$ and

similar for Y . Substituting the projector expansion into Eq. (S3) yields:

$$\begin{aligned}
M_3 &= (\Pi_{+y}^{(1)} - \Pi_{-y}^{(1)}) \otimes (\Pi_{+x}^{(2)} - \Pi_{-x}^{(2)}) \otimes (\Pi_{+x}^{(3)} - \Pi_{-x}^{(3)}) + (\Pi_{+x}^{(1)} - \Pi_{-x}^{(1)}) \otimes (\Pi_{+y}^{(2)} - \Pi_{-y}^{(2)}) \otimes (\Pi_{+x}^{(3)} - \Pi_{-x}^{(3)}) \\
&\quad + (\Pi_{+x}^{(1)} - \Pi_{-x}^{(1)}) \otimes (\Pi_{+x}^{(2)} - \Pi_{-x}^{(2)}) \otimes (\Pi_{+y}^{(3)} - \Pi_{-y}^{(3)}) - (\Pi_{+y}^{(1)} - \Pi_{-y}^{(1)}) \otimes (\Pi_{+y}^{(2)} - \Pi_{-y}^{(2)}) \otimes (\Pi_{+y}^{(3)} - \Pi_{-y}^{(3)}) \\
&= \left(\begin{aligned}
&\Pi_{-y}^{(1)}\Pi_{+y}^{(2)}\Pi_{+y}^{(3)} + \Pi_{-y}^{(1)}\Pi_{-y}^{(2)}\Pi_{-y}^{(3)} + \Pi_{+y}^{(1)}\Pi_{+y}^{(2)}\Pi_{-y}^{(3)} + \Pi_{+y}^{(1)}\Pi_{-y}^{(2)}\Pi_{+y}^{(3)} \\
&+ \Pi_{+y}^{(1)}\Pi_{+x}^{(2)}\Pi_{+x}^{(3)} + \Pi_{+y}^{(1)}\Pi_{-x}^{(2)}\Pi_{-x}^{(3)} + \Pi_{-y}^{(1)}\Pi_{+x}^{(2)}\Pi_{-x}^{(3)} + \Pi_{-y}^{(1)}\Pi_{-x}^{(2)}\Pi_{+x}^{(3)} \\
&+ \Pi_{-x}^{(1)}\Pi_{+y}^{(2)}\Pi_{-x}^{(3)} + \Pi_{-x}^{(1)}\Pi_{-y}^{(2)}\Pi_{+x}^{(3)} + \Pi_{+x}^{(1)}\Pi_{+y}^{(2)}\Pi_{+x}^{(3)} + \Pi_{+x}^{(1)}\Pi_{-y}^{(2)}\Pi_{-x}^{(3)} \\
&+ \Pi_{+x}^{(1)}\Pi_{+x}^{(2)}\Pi_{+y}^{(3)} + \Pi_{+x}^{(1)}\Pi_{-x}^{(2)}\Pi_{-y}^{(3)} + \Pi_{-x}^{(1)}\Pi_{+x}^{(2)}\Pi_{-y}^{(3)} + \Pi_{-x}^{(1)}\Pi_{-x}^{(2)}\Pi_{+y}^{(3)}
\end{aligned} \right) \\
&\quad - \left(\begin{aligned}
&\Pi_{+y}^{(1)}\Pi_{-y}^{(2)}\Pi_{-y}^{(3)} + \Pi_{+y}^{(1)}\Pi_{+y}^{(2)}\Pi_{+y}^{(3)} + \Pi_{-y}^{(1)}\Pi_{-y}^{(2)}\Pi_{+y}^{(3)} + \Pi_{-y}^{(1)}\Pi_{+y}^{(2)}\Pi_{-y}^{(3)} \\
&+ \Pi_{-y}^{(1)}\Pi_{-x}^{(2)}\Pi_{-x}^{(3)} + \Pi_{-y}^{(1)}\Pi_{+x}^{(2)}\Pi_{+x}^{(3)} + \Pi_{+y}^{(1)}\Pi_{-x}^{(2)}\Pi_{+x}^{(3)} + \Pi_{+y}^{(1)}\Pi_{+x}^{(2)}\Pi_{-x}^{(3)} \\
&+ \Pi_{+x}^{(1)}\Pi_{-y}^{(2)}\Pi_{+x}^{(3)} + \Pi_{+x}^{(1)}\Pi_{+y}^{(2)}\Pi_{-x}^{(3)} + \Pi_{-x}^{(1)}\Pi_{-y}^{(2)}\Pi_{-x}^{(3)} + \Pi_{-x}^{(1)}\Pi_{+y}^{(2)}\Pi_{+x}^{(3)} \\
&+ \Pi_{-x}^{(1)}\Pi_{-x}^{(2)}\Pi_{-y}^{(3)} + \Pi_{-x}^{(1)}\Pi_{+x}^{(2)}\Pi_{+y}^{(3)} + \Pi_{+x}^{(1)}\Pi_{-x}^{(2)}\Pi_{+y}^{(3)} + \Pi_{+x}^{(1)}\Pi_{+x}^{(2)}\Pi_{-y}^{(3)}
\end{aligned} \right). \tag{S4}
\end{aligned}$$

By comparing Eq. (S4) with the definition of μ_n in the main text, we immediately find the composing projectors of μ_3 are those projectors with an orange color. We shall define the sixteen projectors as Π_1, \dots, Π_{16} , respectively, so that:

$$\mu_3 = \sum_{k=1}^{16} \langle \Pi_k \rangle. \tag{S5}$$

Note we have rearranged the projectors in the second equality of Eq. (S4). The purpose of doing so is to let the graph of exclusivity have better symmetry.

We are now ready to extract the relation of exclusivity and the graph of exclusivity from the set of projectors. Two projectors Π_i and Π_j are exclusive if $\Pi_i\Pi_j = 0$; for the projectors in the definition of μ_3 , they are the pairs containing Π_{+x} and Π_{-x} (or Π_{+y} and Π_{-y}) acting on the same qubit, so they are bound not to give outcome +1 in the same round of experiment no matter what state is being tested. By applying this rule on the set of projectors, we find the pairs of indices (i, j) , $i < j$ of exclusive projectors, and thus the edge set of the graph of exclusivity, G_3 , to be:

$$\begin{aligned}
V(G_3) &= \{(1, 2), (1, 3), (1, 4), (1, 5), (1, 6), (1, 10), (1, 12), (1, 14), (1, 15), (2, 3), (2, 4), (2, 5), (2, 6), (2, 9), \\
&\quad (2, 11), (2, 13), (2, 16), (3, 4), (3, 7), (3, 8), (3, 10), (3, 12), (3, 13), (3, 16), (4, 7), (4, 8), (4, 9), (4, 11), \\
&\quad (4, 14), (4, 15), (5, 6), (5, 7), (5, 8), (5, 9), (5, 12), (5, 14), (5, 16), (6, 7), (6, 8), (6, 10), (6, 11), \\
&\quad (6, 13), (6, 15), (7, 8), (7, 10), (7, 11), (7, 14), (7, 16), (8, 9), (8, 12), (8, 13), (8, 15), (9, 10), (9, 11), \\
&\quad (9, 12), (9, 13), (9, 14), (10, 11), (10, 12), (10, 13), (10, 14), (11, 12), (11, 15), (11, 16), \\
&\quad (12, 15), (12, 16), (13, 14), (13, 15), (13, 16), (14, 15), (14, 16), (15, 16)\} \tag{S6}
\end{aligned}$$

The edge set induces the graph of exclusivity, G_3 in Fig.1 in the main text. It is the graph complement of the Shrikhande graph. We also redraw the graph of exclusivity in Fig.S1 in this Supplemental Material. By explicitly checking the graph constants of G_3 , we found that $\alpha(G_3) = 3$ and $\vartheta(G_3) = 4$, thus recovering all affirmations in the Eq. (2) in the main text.

Appendix C: Logical contextuality from the graph states

The graph states [4] form a family of highly entangled multipartite state, they can be represented using undirected, connected graphs. In the graph representation \mathcal{G} of a graph state, every qubit is denoted by a vertex, and the connectivity of the graph determines the structure of entanglement. More specifically, let the adjacency matrix of the representation of the graph state be $C(\mathcal{G})$, then the stabilizing operator for each of the qubits are defined as:

$$S^{(j)} \equiv X^{(j)} \prod_{k=1}^n (Z^{(k)})^{C_{jk}}. \quad (\text{S1})$$

Note that, following the convention of Reference [4], we will state all the definitions and proofs using the Pauli operators, but it is also possible to establish the results in a device-independent manner like in the main text. A graph state $|\mathcal{G}\rangle$ is in turn defined as the common +1 eigenstate of all its stabilizing operators:

$$S^{(j)} |\mathcal{G}\rangle = |\mathcal{G}\rangle, \quad \forall j \in \{1, \dots, n\}.$$

A GHZ-type paradox for nonlocality is a contradiction between local hidden-variable theory and the quantum theory upon the measurement result for some dichotomic (± 1) observables, where their prediction about the product of these observables disagree with each other: -1 vs. $+1$. An observation of a GHZ-type paradox with the result in favor of quantum theory serves as a strong proof of quantum nonlocality. For every graph state with at least one universal vertex in its graph representation, a GHZ-type paradox can be formulated using the products of some stabilizing operators [1]. For self-containment, we briefly repeat the construction for an n -qubit graph state where n is odd: let the universal vertex be labeled as 1, then a GHZ-type paradox can be formulated with the following operators:

$$S^{(1)}, \quad S^{(1)\theta(n)} S^{(2)}, \quad \left\{ S^{(1)\theta(j)} S^{(j)} S^{(j+1)} \mid j \in \{2, \dots, n-1\} \right\}, \quad S^{(1)\theta(n)} S^{(n)}, \quad (\text{S2})$$

with $\theta(j) = 1 + C_{n2} + \sum_{k=2, k \neq j}^{n-1} C_{k(k+1)}$. The product of these $m+1$ operators evaluates to -1 and $+1$ in local hidden-variable and quantum theories, therefore manifesting a GHZ-type paradox.

We now turn to investigate the exclusivity structure behind the measurements in (S2). Notice that these observables can also be expressed using individual events, i.e., projective measurements. By normalization of probabilities, the projectors onto the +1 eigenstates of the observables suffices to demonstrate the GHZ-type paradox. Let us denote the set of 2^{n-1} projectors corresponding to the k -th observables in (S2) by $\mathcal{E}_k = \{E_{k1}, E_{k2}, \dots, E_{k(2^{n-1})}\}$, and the graph of exclusivity corresponds to the assemblage of events $\mathfrak{E} = \{\mathcal{E}_1, \mathcal{E}_2, \dots, \mathcal{E}_{n+1}\}$ by G (not to be confused with the calligraphic \mathcal{G} denoting the graph state itself). The graph G has an order of $|V(G)| = (n+1)2^{n-1}$, and the graph constants of interest are the independence number $\alpha(G) = n$ and the Lovász number $\vartheta(G) = n+1$.

Our main goal in this section is to prove the exclusivity graph G can be embedded in a $2^n - 1$ -dimensional Hilbert space, which nonetheless still supports a logical proof of contextuality with a success probability of 1 to trigger a set of events defying noncontextuality. To this aim, it suffices to prove the +1 eigenstates of the projectors in \mathfrak{E} spans a Hilbert space with a dimension of only $2^n - 1$, so it can be related to a set of $2^n - 1$ -dimensional vectors by a unitary isomorphism. The rest of proof exploits a result in Clifford algebra.

Lemma. *Applying Pauli operator σ_z on the j -th qubit of a graph state inverts only the sign of the eigenvalue of the stabilizing operator $S^{(j)}$, and leave the eigenvalues of other stabilizing operator invariant.*

Proof. The expectation values of the stabilizing operators on the σ_z -modified graph state read

$$\left\langle S^{(j)} \right\rangle_{Z^{(k)}|\mathcal{G}\rangle} = \text{Tr} \left(S^{(j)} Z^{(k)} |\mathcal{G}\rangle \langle \mathcal{G}| Z^{(k)} \right) = \text{Tr} \left(Z^{(k)} S^{(j)} Z^{(k)} |\mathcal{G}\rangle \langle \mathcal{G}| \right).$$

From the definition of the graph state and the stabilizing operator (S1), direct calculation shows

$$Z^{(k)} S^{(j)} Z^{(k)} = (1 - 2\delta_{jk}) S^{(j)}.$$

Where δ_{jk} is the Kronecker- δ . Substituting the last relation into the expectation values yields the desired proposition. \square

Because all stabilizing operators for a graph state commute, it is straightforward to check that modulating $|\mathcal{G}\rangle$ with σ_z on different qubits can alternate the signs of the eigenvalues of all stabilizing operators one-by-one.

The above Lemma shows there exist a σ_z -modified graph state,

$$|\tilde{\mathcal{G}}\rangle = \bigotimes_{j=1}^n (Z^{(j)})^{f(j)} \cdot |\mathcal{G}\rangle, \quad (\text{S3})$$

where $f(j) \in \{0, 1\}$, that is the common -1 eigenstate of all the operators in (S2). This is because for all but the last operator a new stabilizing operator appears in every new term, so iterative application of the Lemma on every qubit can guarantee every of the first n operators has an eigenvalue of -1 for the properly modified graph state via a Gaussian elimination over $f(j)$. Finally, observe every stabilizing operator appears in (S2) even times, the last operator must evaluate to -1 in order to keep the product, that is the eigenvalue of an identity matrix, positive.

Using the conversion between events probabilities and operator expectations, we arrive at $\text{Tr}(E_{kl} |\tilde{\mathcal{G}}\rangle \langle \tilde{\mathcal{G}}|) = 0, \forall k \in \{1, \dots, n+1\}, l \in \{1, \dots, 2^{n-1}\}$. As such the following equivalent statements hold: (1) the solution space for $\mathfrak{C}\mathbf{x} = \mathbf{0}$ has the dimension of 1, (2) the projectors \mathfrak{C} has a rank deficiency, and (3) the graph of exclusivity G supports vector realization in $2^n - 1$ -dimensions that manifests a logical noncontextuality paradox. This completes our proof for the logical contextuality originated from the graph states applicable in lower dimensional indivisible systems.

An important merit of the construction here is it secures a 100% success probability of observing the events violating noncontextuality, as opposed to previous Hardy-type contextuality [5, 22] and nonlocality proofs [6–9], where the success probabilities are less than unity and, even less than the fractional parts of the corresponding Bell and noncontextuality inequalities [10–12, 15], due to the setting for maximal violation of the inequalities fail to saturate probabilities of individual cliques. As stated in the main text, the ideal success probability paves the way for a robust experimental observation of logical contextuality in high-dimensional systems.

Appendix D: Direct proof of the logical contextuality (3) in the main text

We show with the following example that the Hardy-type contextuality corresponding to the exclusivity graph in Fig. S1 (same as the Fig. 1 in the main text) admits a logical proof. The proof can be constructed by saturation of subsets of exclusive probabilities; in a similar vein, the proof works for all Hardy-type contextuality with a 100% success probability. Here in our case, the Hardy-like proof of contextuality can be explicitly stated by

$$\begin{aligned} \sum_{i=1}^4 p_i &= 1, \\ \sum_{i=5}^8 p_i &= 1, \\ \sum_{i=9}^{12} p_i &= 1, \\ \hline \sum_{i=13}^{16} p_i &\stackrel{\text{NCHV}}{=} 0. \end{aligned} \quad (\text{S1})$$

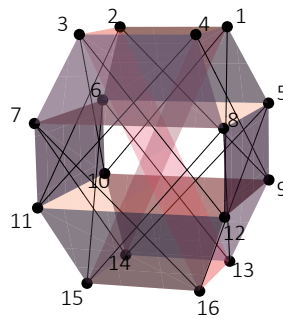


Fig. S1. The 16 vertices represent 16 events. The points connected by a line denote exclusive events, and the four events represented by points on a colored quadrilateral are mutually exclusive.

Proof.—The graph of exclusivity in Fig. S1 is isomorphic to the strongly regular Shrikhande graph. Let us assume that the first three conditions in (S1) are satisfied. In the NCHV theory, the first condition in (S1) implies that there exists one and only one p_i being 1 and others being 0, i.e., one and only one measurement direction in $\{|v_i\rangle : i = 1, 2, 3, 4\}$ with outcome 1. In the following, we start the case study.

(a) If $p_1 = 1$, then the outcome of measurement direction $|v_1\rangle$ is 1. The orthogonality relationships $|v_1\rangle \perp |v_5\rangle, |v_6\rangle, |v_{10}\rangle, |v_{12}\rangle, |v_{14}\rangle, |v_{15}\rangle$ result that all outcomes of measurement directions $|v_5\rangle, |v_6\rangle, |v_{10}\rangle, |v_{12}\rangle, |v_{14}\rangle, |v_{15}\rangle$ must be 0, i.e., $p_5 = p_6 = p_{10} = p_{12} = p_{14} = p_{15} = 0$. Thus, the second (third) condition in (S1) yields that $p_7 + p_8 = 1$ ($p_9 + p_{11} = 1$), i.e., the sum of the outcomes of $|v_7\rangle$ and $|v_8\rangle$ (the sum of the outcomes of $|v_9\rangle$ and $|v_{11}\rangle$) is 1.

(a₁) If the outcome of measurement direction $|v_7\rangle$ is 1, then the outcome of $|v_{11}\rangle$ must be 0 by the orthogonality relationship $|v_7\rangle \perp |v_{11}\rangle$, and so $|v_9\rangle$'s outcome must be 1 by the third condition $p_9 + p_{11} = 1$. Since $|v_{13}\rangle \perp |v_9\rangle, |v_{14}\rangle \perp |v_1\rangle, |v_{15}\rangle \perp |v_1\rangle, |v_{16}\rangle \perp |v_7\rangle$, and all outcomes of $|v_1\rangle, |v_7\rangle, |v_9\rangle$ are 1, we obtain that the outcome of $|v_i\rangle$ ($i = 13, 14, 15, 16$) is 0, i.e., $p_{13} + p_{14} + p_{15} + p_{16} = 0$.

(a₂) If the outcome of measurement direction $|v_8\rangle$ is 1, then the outcome of $|v_9\rangle$ must be 0 by the orthogonality relationship $|v_8\rangle \perp |v_9\rangle$, and so $|v_{11}\rangle$'s outcome must be 1 by the third condition $p_9 + p_{11} = 1$. Since $|v_{13}\rangle \perp |v_8\rangle$, $|v_{14}\rangle \perp |v_1\rangle$, $|v_{15}\rangle \perp |v_1\rangle$, $|v_{16}\rangle \perp |v_{11}\rangle$, and all outcomes of $|v_1\rangle, |v_8\rangle, |v_{11}\rangle$ are 1, we obtain that the outcome of $|v_i\rangle$ ($i = 13, 14, 15, 16$) is 0, i.e., $p_{13} + p_{14} + p_{15} + p_{16} = 0$.

Due to the vertex transitivity of the graph, for the other cases: (b) $p_2 = 1$, (c) $p_3 = 1$, and (d) $p_4 = 1$, we can obtain $p_{13} + p_{14} + p_{15} + p_{16} = 0$. Therefore, in the NCHV theory, the first three conditions in (S1) lead to $p_{13} + p_{14} + p_{15} + p_{16} = 0$. \square

Appendix E: Experimental details

Analytical settings of projectors.— Our experimental settings for realizing the maximal quantum violation of non-contextuality inequality (2) and observing the logical contextuality (3) in the main text are summarized in Table I. Here, $|\psi\rangle$ is the initial state and $|v_i\rangle$ represent the +1-eigenstate of the i -th projector. In other words, the projectors used in the experiment and the rays in the table are related via $\Pi_i = |v_i\rangle\langle v_i|$. The other state preparations and measurement rays required in the experiment were all calculated from the rays listed in the table. Concretely, the full sets of compatible measurements from every four projectors were constructed by introducing extra projectors according to the symmetric form of the existing projectors, and when the projector Π_i giving outcome 0 the post-measurement state was re-prepared as $(\mathbb{I} - \Pi_i)|\psi\rangle$ according to the Lüders rule.

Table I. Optimal measurement settings $|v_i\rangle$ and input state $|\psi\rangle$ for realizing the maximal quantum violation of noncontextuality inequality (2) and observing the logical contextuality (3) in the main text in the 7-dimensional space.

$ v_i\rangle$	i_1	i_2	i_3	i_4	i_5	i_6	i_7	$ v_i\rangle$	i_1	i_2	i_3	i_4	i_5	i_6	i_7
$ v_1\rangle$	1	0	0	0	0	0	0	$ v_9\rangle$	1/2	0	1/2	0	1/√8	-1/√8	1/2
$ v_2\rangle$	0	1	0	0	0	0	0	$ v_{10}\rangle$	0	1/2	0	1/2	-1/√8	1/√8	1/2
$ v_3\rangle$	0	0	1	0	0	0	0	$ v_{11}\rangle$	1/2	0	1/2	0	-1/√8	1/√8	-1/2
$ v_4\rangle$	0	0	0	1	0	0	0	$ v_{12}\rangle$	0	1/2	0	1/2	1/√8	-1/√8	-1/2
$ v_5\rangle$	0	0	1/2	1/2	0	1/√2	0	$ v_{13}\rangle$	1/2	0	0	1/2	1/√8	1/√8	-1/2
$ v_6\rangle$	0	0	1/2	1/2	0	-1/√2	0	$ v_{14}\rangle$	0	1/2	1/2	0	-1/√8	-1/√8	-1/2
$ v_7\rangle$	1/2	1/2	0	0	1/√2	0	0	$ v_{15}\rangle$	0	1/2	1/2	0	1/√8	1/√8	1/2
$ v_8\rangle$	1/2	1/2	0	0	-1/√2	0	0	$ v_{16}\rangle$	1/2	0	0	1/2	-1/√8	-1/√8	1/2
								$ \psi\rangle$	1/2	1/2	1/2	1/2	0	0	0

Estimation of counting errors in the experiment.— The data in our experiment were registered with a single-photon avalanche detector, and the counting rate was about 10^5 /s when the preparation and measurement basis were aligned. As the counting events occurred randomly in time, but were independent of each other and identically distributed, the statistics of photon counting must follow a Poissonian distribution. To estimate the uncertainty of our data collection process, we took the registered number of counting events as the expectation of the Poissonian distribution, and resampled the numbers in a `Mathematica` program. We used the resampled data to generate 100 groups of detection event probabilities, which were further used to calculate the expectations of all the observables required in the experiment. The standard deviations of these expectations were taken as the 1σ error bars of the corresponding observables.

Calibration of preparations and measurements.— To benchmark the performance of our prepare-and-measure setup, we prepared the initial state and the +1-eigenstates of all the projectors that appeared in the experiment using the first and the second spatial light modulator (SLM), respectively, according to the analytical settings in Table I, and measured the beam profile at the focal plane conjugate to the second SLM using a charge-coupled device camera. Here, the projectors' +1-eigenstates were used to calibrate the performance of the measurements implemented by the projectors. In both cases, the other SLM displayed a blazed grating with maximal contrast to keep the optical path unchanged and maximize the optical power at the camera. In Table II, we report the Pearson correlations between the beam profiles corresponding to the state/projectors measured and the ideal intensity distribution.

Appendix F: Data analysis

Observation of the Hardy-type contextuality.— We begin the data analysis by observing the Hardy-type contextuality in Eq. (3) of the main text. To this aim, only the detection probabilities of the initial state on the +1-eigenstate of the 16 projectors in Table I are required; these values, together with the sum of the probabilities corresponding to the projectors in the same context, are listed in Table III. The recorded probabilities give:

$$\sum_{k=1}^4 P(1|k) = 0.9906, \quad \sum_{k=5}^8 P(1|k) = 0.9861, \quad \sum_{k=9}^{12} P(1|k) = 0.9816, \quad \sum_{k=13}^{16} P(1|k) = 0.9768. \quad (\text{S1})$$

We see that the first three probabilities agree with the three constraints in Eq. (3) well, and the fourth probability strongly favors the prediction of quantum mechanics over the noncontextuality theories. If we look at the sum of all the probabilities, we still have $\sum_{k=1}^{16} P(1|k) = 3.9351$ exceeding the classical budget given by taking the sum of the probabilities in Eq. (3) and assume the noncontextuality prediction; in contrast, the total probability only falls short of the quantum prediction by 0.0649 due to experimental imperfections like dark counts and finite extinction ratio of projective measurements.

Our purpose of observing the Hardy-type paradox here was to establish the picture of logical contextuality and intuitively demonstrate the inconsistency between the predictions of noncontextuality and quantum theories. A quantified test of the paradox would rely on the condition that all the relations of orthogonality, as specified by the graph of exclusivity, strictly hold, which was never the case experimentally. For the same reason, we did not analyze the statistical significance of the observed Hardy-type paradox; the high-dimensional contextuality will be quantified using the contextuality witness in the next section.

Calculation of the contextuality witness μ_3 .— We used the noncontextuality inequality Eq. (4) in the main text to quantify the degree of contextuality in our experiment. The terms on the left-hand side of the inequality only consist of two types of probabilities: (i) $\{P(1|k) \mid k \in V(G_3)\}$, the detection probabilities of the initial state on the +1-eigenstate of the 16 projectors that already appeared in Table III, and (ii) $\{P(1, 1|i, j) \mid (i, j) \in E(G_3)\}$, the probabilities of two ideally exclusive projective measurements both give result 1 when implemented sequentially. Experimentally, these probabilities were determined by the decomposition of sequential measurements into demolition measurements and the reparation of post-measurement states, which gives:

$$P(1, 1|i, j) = P(1|i) P(1|i = 1, j), \quad (\text{S2})$$

where $P(1|i = 1, j)$ indicates the detection probability of the +1-eigenstate of $\Pi_i = |v_i\rangle\langle v_i|$ (that is, the post-measurement state when the outcome of Π_i is 1) on the +1-eigenstate of $\Pi_j = |v_j\rangle\langle v_j|$. By this decomposition, we were able to calculate all the probabilities in Eq. (4) in the main text using the recorded probabilities $P(1|i)$ as given in Table III and $P(1|i = 1, j)$ as given in Table IV. Our results gave $\mu_3 \geq 3.821 \pm 0.012$ violating the prediction of noncontextuality by 68.7 standard deviations. Comparing the ratio between the experimental result

Table II. Experimentally prepared beam profiles, theoretical predictions, and the Pearson correlations between pairs of images.

Ray	$ v_1\rangle$	$ v_2\rangle$	$ v_3\rangle$	$ v_4\rangle$	$ v_5\rangle$	$ v_6\rangle$
Theory						
Experiment						
Pearson correlation	95.96%	95.86%	95.75%	95.75%	94.71%	94.79%

Continued on next page →

Table II. (continue)

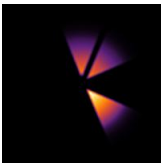
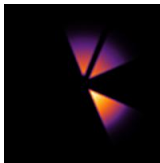




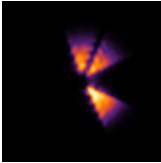
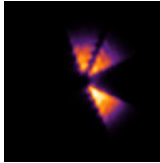
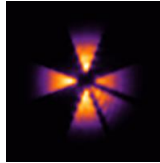
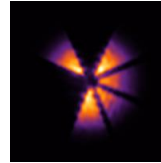
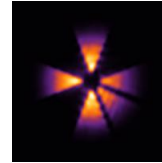
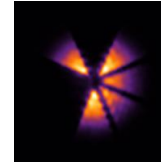
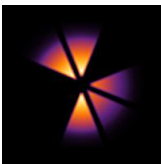
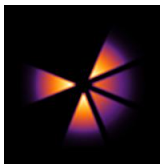



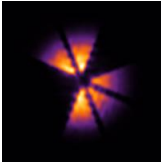
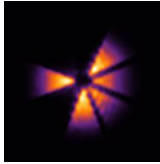
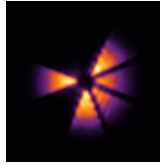
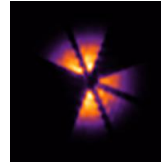
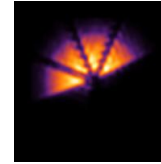
Vector	$ v_7\rangle$	$ v_8\rangle$	$ v_9\rangle$	$ v_{10}\rangle$	$ v_{11}\rangle$	$ v_{12}\rangle$
Theory						
Experiment						
Pearson correlation	95.28%	95.24%	95.53%	95.07%	94.99%	94.67%
Vector	$ v_{13}\rangle$	$ v_{14}\rangle$	$ v_{15}\rangle$	$ v_{16}\rangle$		$ \psi\rangle$
Theory						
Experiment						
Pearson correlation	95.16%	95.31%	95.91%	95.64%		95.82%
Average Pearson correlation						95.46%

Table III. Recorded detection probabilities of the initial state $|\psi\rangle = (|1\rangle + |2\rangle + |3\rangle + |4\rangle)/2$ on various projectors defined in Table I. These probabilities establish the Hardy-type argument in Eq. (3) in the main text—the sum of all the probabilities markedly exceeded the budget allowed by any classical (noncontextuality) theory and was close to the prediction of quantum theory. The statistical significance of the data in the “subtotal” and “total” columns are not analyzed because the projectors in each context did not have ideal exclusivity; that is, the observed Hardy-type contextuality was qualitative.

Context	Term	Measured result	Term	Measured result	Term	Measured result	Term	Measured result	Subtotal
1	$P(1 1)$	0.2384 ± 0.0014	$P(1 2)$	0.2534 ± 0.0014	$P(1 3)$	0.2415 ± 0.0014	$P(1 4)$	0.2574 ± 0.0014	0.9906
2	$P(1 5)$	0.2585 ± 0.0015	$P(1 6)$	0.2410 ± 0.0014	$P(1 7)$	0.2512 ± 0.0014	$P(1 8)$	0.2353 ± 0.0014	0.9861
3	$P(1 9)$	0.2439 ± 0.0014	$P(1 10)$	0.2536 ± 0.0014	$P(1 11)$	0.2431 ± 0.0014	$P(1 12)$	0.241 ± 0.0014	0.9816
4	$P(1 13)$	0.2337 ± 0.0014	$P(1 14)$	0.2437 ± 0.0014	$P(1 15)$	0.2538 ± 0.0014	$P(1 16)$	0.2456 ± 0.0014	0.9768
Total									3.9351
Classical budget									3
Quantum prediction									4

and the noncontextuality bound, we found a ratio of $\mu_3/\alpha \geq 1.273$. To our best knowledge, this is the largest quantum–classical ratio ever reported in a single-particle test of contextuality; see Section G for a corroboration.

Verification of the no-signaling condition.— Although the nullification test of the signaling factors does not affect the values of the contextuality witness, it is nonetheless crucial for revealing the failure of the noncontextuality models and understanding the experiment: doing a test of contextuality means we are testing against the noncontextual

Table IV. Joint detection probabilities of exclusive projectors. The probability $P(1|i=1, j)$ indicates the detection probability of the +1-eigenstate of $\Pi_i = |v_i\rangle\langle v_i|$ (that is, the post-measurement state when the outcome of Π_i is 1) on the +1-eigenstate of $\Pi_j = |v_j\rangle\langle v_j|$. We would have $\Pi_i\Pi_j = 0$ across any row of the table if the conditions of orthogonality, given by the graph of exclusivity, are strict. The non-zero values thus indicate deviations from ideal exclusivity and were exploited to bound the value of the contextuality witness μ_3 using the inequality (4) in the main text.

Index	Edge (i, j)	$P(1 i=1, j)$ (%)	$P(1 j=1, i)$ (%)	Index	Edge (i, j)	$P(1 i=1, j)$ (%)	$P(1 j=1, i)$ (%)
1	(1, 2)	1.211 ± 0.031	1.079 ± 0.030	37	(5, 16)	0.995 ± 0.028	1.150 ± 0.030
2	(1, 3)	0.053 ± 0.007	0.093 ± 0.009	38	(6, 7)	0.151 ± 0.011	0.268 ± 0.015
3	(1, 4)	0.036 ± 0.005	0.062 ± 0.007	39	(6, 8)	0.239 ± 0.014	0.420 ± 0.018
4	(1, 5)	0.161 ± 0.011	0.067 ± 0.007	40	(6, 10)	1.154 ± 0.031	1.131 ± 0.030
5	(1, 6)	0.126 ± 0.010	0.040 ± 0.006	41	(6, 11)	0.902 ± 0.027	0.971 ± 0.028
6	(1, 10)	1.261 ± 0.032	1.674 ± 0.037	42	(6, 13)	1.163 ± 0.031	1.323 ± 0.033
7	(1, 12)	0.264 ± 0.015	0.411 ± 0.018	43	(6, 15)	1.031 ± 0.029	0.995 ± 0.028
8	(1, 14)	0.229 ± 0.014	0.158 ± 0.011	44	(7, 8)	0.344 ± 0.017	0.260 ± 0.015
9	(1, 15)	1.536 ± 0.035	1.188 ± 0.031	45	(7, 10)	0.951 ± 0.028	0.639 ± 0.023
10	(2, 3)	0.699 ± 0.024	0.807 ± 0.026	46	(7, 11)	0.597 ± 0.022	0.512 ± 0.020
11	(2, 4)	0.040 ± 0.006	0.071 ± 0.008	47	(7, 14)	0.283 ± 0.015	0.387 ± 0.018
12	(2, 5)	0.203 ± 0.013	0.250 ± 0.014	48	(7, 16)	0.587 ± 0.022	0.568 ± 0.021
13	(2, 6)	0.469 ± 0.019	0.441 ± 0.019	49	(8, 9)	0.330 ± 0.016	0.464 ± 0.019
14	(2, 9)	0.318 ± 0.016	0.493 ± 0.020	50	(8, 12)	0.269 ± 0.015	0.285 ± 0.015
15	(2, 11)	0.384 ± 0.018	0.442 ± 0.019	51	(8, 13)	0.648 ± 0.023	0.619 ± 0.022
16	(2, 13)	0.619 ± 0.022	0.493 ± 0.020	52	(8, 15)	0.558 ± 0.021	0.634 ± 0.023
17	(2, 16)	0.815 ± 0.026	0.388 ± 0.018	53	(9, 10)	1.180 ± 0.031	0.991 ± 0.028
18	(3, 4)	1.475 ± 0.035	1.526 ± 0.035	54	(9, 11)	0.665 ± 0.023	0.608 ± 0.022
19	(3, 7)	0.222 ± 0.013	0.375 ± 0.017	55	(9, 12)	0.340 ± 0.017	0.209 ± 0.013
20	(3, 8)	0.375 ± 0.017	0.378 ± 0.017	56	(9, 13)	0.507 ± 0.020	0.509 ± 0.020
21	(3, 10)	0.767 ± 0.025	0.803 ± 0.025	57	(9, 14)	0.521 ± 0.021	0.745 ± 0.025
22	(3, 12)	0.434 ± 0.019	0.547 ± 0.021	58	(10, 11)	0.759 ± 0.025	0.832 ± 0.026
23	(3, 13)	0.737 ± 0.024	0.669 ± 0.023	59	(10, 12)	0.504 ± 0.020	0.646 ± 0.023
24	(3, 16)	0.878 ± 0.027	0.513 ± 0.020	60	(10, 13)	1.232 ± 0.032	0.864 ± 0.026
25	(4, 7)	0.509 ± 0.020	0.400 ± 0.018	61	(10, 14)	0.406 ± 0.018	0.326 ± 0.016
26	(4, 8)	0.568 ± 0.021	0.374 ± 0.017	62	(11, 12)	0.423 ± 0.018	0.291 ± 0.015
27	(4, 9)	1.074 ± 0.029	1.064 ± 0.029	63	(11, 15)	1.026 ± 0.029	0.838 ± 0.026
28	(4, 11)	0.692 ± 0.024	0.632 ± 0.023	64	(11, 16)	0.222 ± 0.013	0.183 ± 0.012
29	(4, 14)	0.673 ± 0.023	0.680 ± 0.023	65	(12, 15)	0.392 ± 0.018	0.456 ± 0.019
30	(4, 15)	0.981 ± 0.028	0.941 ± 0.028	66	(12, 16)	0.508 ± 0.020	0.643 ± 0.023
31	(5, 6)	1.699 ± 0.037	2.147 ± 0.042	67	(13, 14)	0.440 ± 0.019	0.395 ± 0.018
32	(5, 7)	0.082 ± 0.008	0.221 ± 0.013	68	(13, 15)	1.192 ± 0.031	1.057 ± 0.029
33	(5, 8)	0.293 ± 0.015	0.298 ± 0.016	69	(13, 16)	0.610 ± 0.022	0.494 ± 0.020
34	(5, 9)	1.001 ± 0.028	1.041 ± 0.029	70	(14, 15)	0.706 ± 0.024	0.846 ± 0.026
35	(5, 12)	1.487 ± 0.035	1.026 ± 0.029	71	(14, 16)	0.043 ± 0.006	0.158 ± 0.011
36	(5, 14)	0.789 ± 0.025	0.961 ± 0.028	72	(15, 16)	1.481 ± 0.035	1.257 ± 0.032

hidden-variable models, in which observables have predefined context-insensitive values. If the measurement of a preceding observable disturbs the probability distribution of the succeeding observable, it can no longer be considered revealing the predefined values of the observables, and the observed phenomenon will not be able to serve as a test of the noncontextuality theory. By implementing the no-signaling test, we showed our measurements in the experiment fulfill the assumptions of no-disturbance in the noncontextuality theory; thus, it is sensible to be considered a test of the theory itself.

To determine the signaling factors, we rewrite the probabilities in Eq. (5) of the main text in terms of prepare-and-

Table V. Detection probabilities of post-measurement states on compatible projectors. The probability $P(1|i=0, j)$ indicates the detection probability of the state $(\mathbb{I} - \Pi_i)|\psi\rangle / \text{Tr}[(\mathbb{I} - \Pi_i)|\psi\rangle\langle\psi|]$ (that is, the post-measurement state of $|\psi\rangle$ when the measurement outcome of Π_i is 0) on the +1-eigenstate of $\Pi_j = |v_j\rangle\langle v_j|$. The theoretical values are 1/3 for all entries across the table. The quantities here, together with those in Table III and IV, were exploited to estimate the value of the signaling factors ε'_{ij} using Eq. (5) in the main text.

Index	Edge (i, j)	$P(1 i=0, j)$ (%)	$P(1 j=0, i)$ (%)	Index	Edge (i, j)	$P(1 i=0, j)$ (%)	$P(1 j=0, i)$ (%)
1	(1, 2)	32.47 ± 1.40	30.37 ± 1.37	37	(5, 16)	36.04 ± 1.39	38.23 ± 1.42
2	(1, 3)	30.88 ± 1.39	28.93 ± 1.37	38	(6, 7)	34.17 ± 1.42	34.08 ± 1.42
3	(1, 4)	35.06 ± 1.42	33.46 ± 1.40	39	(6, 8)	29.36 ± 1.38	32.02 ± 1.42
4	(1, 5)	33.67 ± 1.40	31.04 ± 1.37	40	(6, 10)	33.58 ± 1.41	32.79 ± 1.39
5	(1, 6)	29.57 ± 1.38	28.86 ± 1.37	41	(6, 11)	28.35 ± 1.36	31.16 ± 1.39
6	(1, 10)	32.13 ± 1.39	29.03 ± 1.36	42	(6, 13)	29.58 ± 1.39	32.16 ± 1.42
7	(1, 12)	31.35 ± 1.40	28.97 ± 1.37	43	(6, 15)	33.14 ± 1.40	31.19 ± 1.37
8	(1, 14)	29.46 ± 1.37	29.90 ± 1.38	44	(7, 8)	33.29 ± 1.40	31.12 ± 1.37
9	(1, 15)	32.86 ± 1.40	29.03 ± 1.36	45	(7, 10)	33.56 ± 1.37	34.49 ± 1.38
10	(2, 3)	33.85 ± 1.38	36.56 ± 1.42	46	(7, 11)	29.76 ± 1.34	31.67 ± 1.36
11	(2, 4)	36.82 ± 1.39	37.22 ± 1.40	47	(7, 14)	33.38 ± 1.38	31.49 ± 1.36
12	(2, 5)	35.23 ± 1.37	35.22 ± 1.37	48	(7, 16)	34.39 ± 1.39	33.73 ± 1.38
13	(2, 6)	33.87 ± 1.38	33.21 ± 1.38	49	(8, 9)	29.19 ± 1.39	28.98 ± 1.38
14	(2, 9)	35.04 ± 1.39	37.06 ± 1.42	50	(8, 12)	28.06 ± 1.38	30.26 ± 1.40
15	(2, 11)	31.43 ± 1.35	32.64 ± 1.36	51	(8, 13)	29.34 ± 1.40	30.49 ± 1.42
16	(2, 13)	32.26 ± 1.38	34.89 ± 1.41	52	(8, 15)	30.44 ± 1.39	28.45 ± 1.36
17	(2, 16)	34.17 ± 1.38	35.96 ± 1.40	53	(9, 10)	34.78 ± 1.41	31.76 ± 1.37
18	(3, 4)	34.59 ± 1.41	33.14 ± 1.39	54	(9, 11)	31.94 ± 1.39	31.44 ± 1.38
19	(3, 7)	33.21 ± 1.40	31.54 ± 1.38	55	(9, 12)	31.48 ± 1.38	33.42 ± 1.41
20	(3, 8)	30.43 ± 1.39	32.82 ± 1.43	56	(9, 13)	30.45 ± 1.38	31.68 ± 1.40
21	(3, 10)	34.54 ± 1.41	32.38 ± 1.38	57	(9, 14)	32.84 ± 1.40	29.55 ± 1.36
22	(3, 12)	31.69 ± 1.40	29.22 ± 1.36	58	(10, 11)	34.71 ± 1.39	34.23 ± 1.38
23	(3, 13)	32.00 ± 1.42	29.65 ± 1.39	59	(10, 12)	31.41 ± 1.35	33.64 ± 1.38
24	(3, 16)	32.16 ± 1.40	32.66 ± 1.40	60	(10, 13)	33.27 ± 1.39	34.62 ± 1.41
25	(4, 7)	33.84 ± 1.35	36.50 ± 1.39	61	(10, 14)	34.43 ± 1.38	33.58 ± 1.38
26	(4, 8)	34.56 ± 1.39	37.33 ± 1.43	62	(11, 12)	27.55 ± 1.34	31.30 ± 1.38
27	(4, 9)	32.97 ± 1.36	33.60 ± 1.36	63	(11, 15)	32.06 ± 1.37	33.66 ± 1.40
28	(4, 11)	32.83 ± 1.36	34.60 ± 1.38	64	(11, 16)	34.52 ± 1.42	29.60 ± 1.36
29	(4, 14)	33.83 ± 1.37	34.59 ± 1.38	65	(12, 15)	31.82 ± 1.38	32.87 ± 1.39
30	(4, 15)	34.87 ± 1.36	36.80 ± 1.39	66	(12, 16)	34.48 ± 1.43	29.03 ± 1.36
31	(5, 6)	34.34 ± 1.38	36.60 ± 1.41	67	(13, 14)	28.33 ± 1.38	29.03 ± 1.39
32	(5, 7)	36.72 ± 1.39	36.13 ± 1.38	68	(13, 15)	31.16 ± 1.40	25.77 ± 1.33
33	(5, 8)	35.34 ± 1.40	36.37 ± 1.41	69	(13, 16)	33.96 ± 1.45	29.38 ± 1.39
34	(5, 9)	35.61 ± 1.39	36.78 ± 1.40	70	(14, 15)	32.32 ± 1.38	33.59 ± 1.39
35	(5, 12)	34.19 ± 1.38	35.25 ± 1.38	71	(14, 16)	32.90 ± 1.40	29.57 ± 1.36
36	(5, 14)	34.53 ± 1.38	33.37 ± 1.36	72	(15, 16)	33.69 ± 1.38	34.55 ± 1.39

measure probabilities using measurement decompositions:

$$\varepsilon_{ij} = P(1|i) - P(1, 1|i, j) - P(1, 0|i, j) = P(1|i) - P(1|i)[P(1|j) + P(0|j)] = 0, \quad (\text{S3})$$

$$\varepsilon'_{ij} = P(1|j) - P(1, 1|i, j) - P(0, 1|i, j) = P(1|j) - P(1|i)P(1|i=1, j) - [1 - P(1|i)]P(1|i=0, j). \quad (\text{S4})$$

Therefore, the factors ε_{ij} signifying the effect of a measurement on its preceding measurement always evaluate to zero. It is expected since no measurement has the effect of signaling backward in time. On the other hand, the factors ε'_{ij} signifying the effect of a measurement on its succeeding measurement are not guaranteed to cancel out, so the

vanish of these factors is nontrivial and indicates no-disturbance between two measurements and the measurements have plausible compatibility.

Calculation of the quantities in Eq. (S4) only requires one more type of probability that is not specified in the previous text. It is $P(1|i = 0, j)$, the detection probability of the state $(\mathbb{I} - \Pi_i) |\psi\rangle / \text{Tr}[(\mathbb{I} - \Pi_i) |\psi\rangle \langle \psi|]$ (that is, the post-measurement state of $|\psi\rangle$ when the measurement outcome of Π_i is 0) on the $+1$ -eigenstate of $\Pi_j = |v_j\rangle \langle v_j|$. The experimental results of $P(1|i = 0, j)$ are given in Table V which, with the other probabilities already given previously, are used to calculate the signaling factors ε'_{ij} in the Fig. 4 of the main text. Our results specifically confirm that the destructive measurement and reparation procedure adopted here, modulo some unavoidable experimental imperfections, does not affect the probability distribution of observables. Therefore, even though we did not use the sequential measurements experimentally, we were still able to assume the Lüders rule, which is itself noncontextual, as the method for reparation of the post-measurement state and test quantum contextuality.

Appendix G: Summary of results: single-particle tests of contextuality

In Fig. S2, we compare the degree of contextuality observed in our experiment with the results of other works reported in the literature [13–33]. The degree of contextuality is quantified by the violation ratio of the noncontextuality inequality in the Cabello–Severini–Winter (sum of event probability) form [2]. The ratio has the physical implication of how much error every individual projective measurement can tolerate before the phenomenon of contextuality disappears; in this way, the results in different experiments can be compared in a consistent sense.

It is evident that the results in different works are presented in different ways, and to make the comparison we need to convert the results into the measurement probability form. Here, we shall use the experimental results reported in Ref. [15] to illustrate how the conversion works.

The noncontextuality inequality tested in Ref. [15] reads:

$$\langle A_1 A_2 \rangle + \langle A_2 A_3 \rangle + \langle A_3 A_4 \rangle + \langle A_4 A_5 \rangle + \langle A_5 A'_1 \rangle - \langle A_1 A'_1 \rangle \stackrel{\text{NCHV}}{\geq} -4, \quad (\text{S1})$$

where the d -dimensional observables A_1, \dots, A_5 and A'_1 have one eigenvalue being -1 and the other $d - 1$ eigenvalues being $+1$. The equation was derived by introducing a correction term to the Klyachko–Can–Binicioğlu–Shumovsky noncontextuality inequality to account for the different realizations of the same measurement in different contexts. The correlations are related to the probabilities of element events by $\langle A_j A_k \rangle = P(A_i = +1, A_j = +1) + P(A_i = -1, A_j = -1) - P(A_i = -1, A_j = +1) - P(A_i = +1, A_j = -1)$. If we only keep the probabilities of element events which *increases* the violation of the inequality, we can exploit the completeness of the probabilities to write:

$$\langle A_j A_k \rangle = 1 - 2 [P(A_i = -1, A_j = +1) - P(A_i = +1, A_j = -1)], \quad (\text{S2})$$

and substituting the above relation into Eq. (S1), which yields:

$$\sum_{k=1}^4 P(A_k = +1, A_{k+1} = -1) + \sum_{k=1}^4 P(A_k = -1, A_{k+1} = +1) + P(A_1 = +1, A'_1 = +1) + P(A_1 = -1, A'_1 = -1) \stackrel{\text{NCHV}}{\leq} 5. \quad (\text{S3})$$

The inequality is but a noncontextuality inequality in the measurement probability form; for this kind of inequality, the noncontextuality bound of the quantum maximum can be determined using the graph-theoretic approach to quantum correlations.

We plot the graph of exclusivity here in Fig. S3. It is an Möbius ladder M_{12} with a length of 6. The independence number of the graph is $\alpha(M_{12}) = 5$ —it is also the classical bound in Eq. (S3). The quantum maximum of Eq. (S3) is the Lovász number of the graph of exclusivity, which was recently proved for the Möbius ladders to be [34]

$$\vartheta(M_{2n}) = \frac{n}{2} \left(1 + \cos \frac{\pi}{n} \right);$$

substituting $n = 6$ into the expression we have $\vartheta(M_{12}) = 3 + 3\sqrt{3}/2 \approx 5.598$. On the experiment side, we use the inverse transformation of Eq. (S2) to calculate the experimental left-hand side value of the inequality (S3) from the data already available in Ref. [15]. We found the reported result achieved a violation ratio of 8.12% against the noncontextuality models.

Using the methods above, we have evaluated the violation of noncontextuality from the other works in the sum of event probability picture. In particular, we calculate the left-hand side value, μ , of the noncontextuality inequality

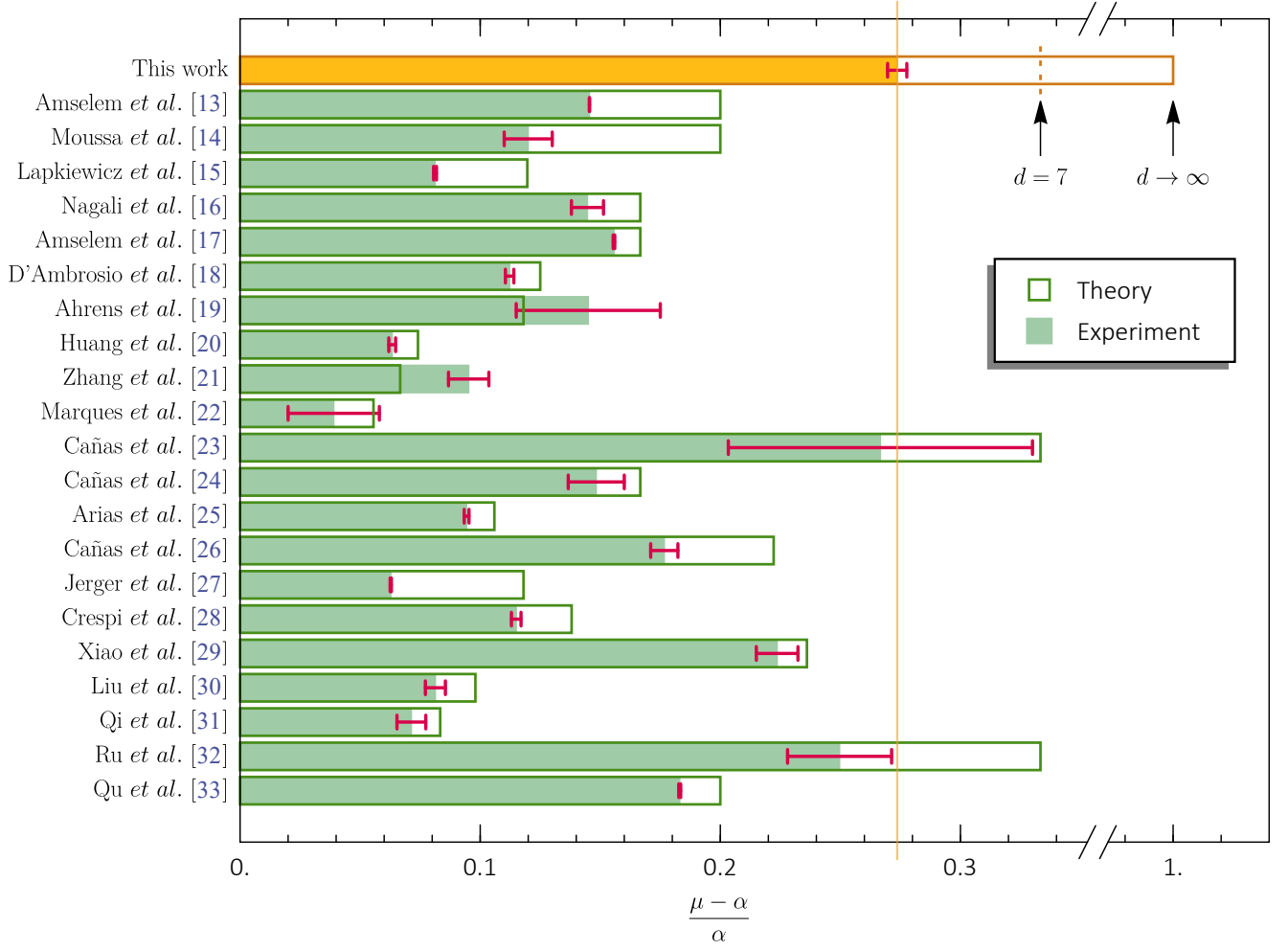


Fig. S2. Comparison of the results in single-particle tests of contextuality, in the present work and from literature [13–33]. The degree of contextuality is quantified by the violation of the noncontextuality inequality in the Cabello–Severini–Winter form normalized by the classical bound. Here, μ indicates the observed left-hand side value of the noncontextuality inequality, and α is the independence number of the graph of exclusivity corresponding to the tested noncontextuality (and thus its classical bound). The error bars represent the 1σ standard deviation of the experimental results. The frame and filling of the bars give the theoretical maximum and experimental results. For the present work, the solid and dashed theoretical bounds correspond to an infinite-dimensional system and a 7-dimensional system, respectively.

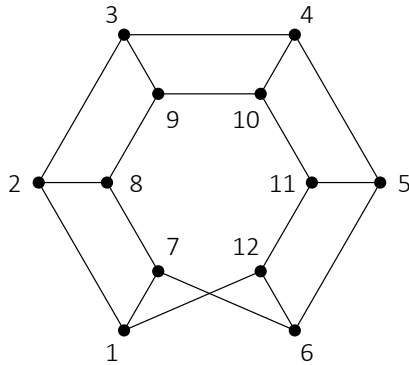


Fig. S3. The graph of exclusivity of the events appeared in Ref. [15]. The definition of the events are: 1: $A_1 = +1, A_2 = -1$, 2: $A_2 = +1, A_3 = -1$, 3: $A_3 = +1, A_4 = -1$, 4: $A_4 = +1, A_5 = -1$, 5: $A_5 = +1, A'_1 = -1$, 6: $A'_1 = +1, A_1 = +1$, 7: $A_1 = -1, A_2 = +1$, 8: $A_2 = -1, A_3 = +1$, 9: $A_3 = -1, A_4 = +1$, 10: $A_4 = -1, A_5 = +1$, 11: $A_5 = -1, A'_1 = +1$, 12: $A'_1 = -1, A_1 = -1$.

in each of the works using the reported results, and use the graph of exclusivity of the measurements to determine the classical bound α and the quantum maximum ϑ . The plotted quantities in Fig. S2 are the experimental ratio of violation of the noncontextuality inequality, $(\mu - \alpha)/\alpha$ and the maximal ratio of violation allowed by the quantum theory, $(\vartheta - \alpha)/\alpha$. We note that in Ref. [13–15] and [19, 21], the reported data were not enough to determine the orthogonality of ideally exclusive measurements, and we did not subtract the effect therein; this causes the latter two works appear to have an observed correlation stronger than the quantum maximum. In Ref. [24, 32], the theoretical bound of violation is the same as the case of $d = 7$ in our work; however, our experiment used a lower Hilbert space dimension than both of the two previous works, and our construction grows stronger when the Hilbert space dimension further increases. Overall, the comparison here corroborated our previous affirmation that the result reported here is the highest degree of contextuality ever observed on a single system.

-
- [1] Z.-H. Liu, J. Zhou, H.-X. Meng, M. Yang, Q. Li, Y. Meng, H.-Y. Su, J.-L. Chen, K. Sun, J.-S. Xu, C.-F. Li, and G.-C. Guo, Experimental test of the Greenberger–Horne–Zeilinger-type paradoxes in and beyond graph states, *npj Quant. Inf.* **7**, 66 (2021).
 - [2] A. Cabello, S. Severini, and A. Winter, Graph-Theoretic Approach to Quantum Correlations, *Phys. Rev. Lett.* **112**, 040401 (2014).
 - [3] A. Cabello, Simple method for experimentally testing any form of quantum contextuality, *Phys. Rev. A* **93**, 032102 (2016).
 - [4] M. Hein, J. Eisert, and H. J. Briegel, Multiparty entanglement in graph states, *Phys. Rev. A* **69**, 062311 (2004).
 - [5] A. Cabello, P. Badziag, M. T. Cunha, and M. Bourennane, Simple Hardy-Like Proof of Quantum Contextuality, *Phys. Rev. Lett.* **111**, 180404 (2013).
 - [6] L. Hardy, Nonlocality for Two Particles without Inequalities for Almost All Entangled States, *Phys. Rev. Lett.* **71**, 1665 (1993).
 - [7] S.-H. Jiang, Z.-P. Xu, H.-Y. Su, A. K. Pati, and J.-L. Chen, Generalized Hardy’s Paradox, *Phys. Rev. Lett.* **120**, 050403 (2018).
 - [8] Y.-H. Luo, H.-Y. Su, H.-L. Huang, X.-L. Wang, T. Yang, L. Li, N.-L. Liu, J.-L. Chen, C.-Y. Lu, and J.-W. Pan, Experimental test of generalized Hardy’s paradox, *Sci. Bull.* **63**, 1611 (2018).
 - [9] M. Yang, H.-X. Meng, J. Zhou, Z.-P. Xu, Y. Xiao, K. Sun, J.-L. Chen, J.-S. Xu, C.-F. Li, and G.-C. Guo, Stronger Hardy-type paradox based on the Bell inequality and its experimental test, *Phys. Rev. A* **99**, 032103 (2019).
 - [10] N. D. Mermin, Quantum mysteries refined, *Am. J. Phys.* **62**, 880 (1994).
 - [11] A. A. Klyachko, M. A. Can, S. Binicioğlu and A. S. Shumovsky, Simple Test for Hidden Variables in Spin-1 Systems, *Phys. Rev. Lett.* **101**, 020403 (2008).
 - [12] M. Sadiq, P. Badziag, M. Bourennane, and A. Cabello, Bell inequalities for the simplest exclusivity graph, *Phys. Rev. A* **87**, 012128 (2013).
 - [13] E. Amsellem, M. Rådmark, M. Bourennane, and A. Cabello, State-independent quantum contextuality with single photons, *Phys. Rev. Lett.* **103**, 160405 (2009).
 - [14] O. Moussa, C. A. Ryan, D. G. Cory, and R. Laflamme, Testing contextuality on quantum ensembles with one clean qubit, *Phys. Rev. Lett.* **104**, 160501 (2010).
 - [15] R. Lapkiewicz, P. Li, C. Schaeff, N. K. Langford, S. Ramelow, M. Wieśniak, and A. Zeilinger, Experimental non-classicality of an indivisible quantum system, *Nature* **474**, 490 (2011).
 - [16] E. Nagali, V. D’Ambrosio, F. Sciarrino, and A. Cabello, Experimental observation of impossible-to-beat quantum advantage on a hybrid photonic system, *Phys. Rev. Lett.* **108**, 090501 (2012).
 - [17] E. Amsellem, L. E. Danielsen, A. J. López-Tarrida, J. R. Portillo, M. Bourennane, and A. Cabello, Experimental fully contextual correlations, *Phys. Rev. Lett.* **108**, 200405 (2012).
 - [18] V. D’Ambrosio, I. Herbauts, E. Amsellem, E. Nagali, M. Bourennane, F. Sciarrino, and A. Cabello, Experimental implementation of a Kochen-Specker set of quantum tests, *Phys. Rev. X* **3**, 011012 (2013).
 - [19] J. Ahrens, E. Amsellem, A. Cabello, and M. Bourennane Two fundamental experimental tests of nonclassicality with qutrits, *Sci. Rep.* **3**, 2170 (2013).
 - [20] Y.-F. Huang, M. Li, D.-Y. Cao, C. Zhang, Y.-S. Zhang, B.-H. Liu, C.-F. Li, and G.-C. Guo, Experimental test of state-independent quantum contextuality of an indivisible quantum system, *Phys. Rev. A* **87**, 052133 (2013).
 - [21] X. Zhang, M. Um, J. Zhang, S. An, Y. Wang, D.-L. Deng, C. Shen, L.-M. Duan, and K. Kim, State-independent experimental test of quantum contextuality with a single trapped ion, *Phys. Rev. Lett.* **110**, 070401 (2013).
 - [22] B. Marques, J. Ahrens, M. Nawareg, A. Cabello, and M. Bourennane, Experimental observation of Hardy-like quantum contextuality, *Phys. Rev. Lett.* **113**, 250403 (2014).
 - [23] G. Cañas, S. Etcheverry, E. S. Gómez, C. Saavedra, G. B. Xavier, G. Lima, and A. Cabello, Experimental implementation of an eight-dimensional Kochen-Specker set and observation of its connection with the Greenberger-Horne-Zeilinger theorem, *Phys. Rev. A* **90**, 012119 (2014).
 - [24] G. Cañas, M. Arias, S. Etcheverry, E. S. Gómez, A. Cabello, G. B. Xavier, and G. Lima, Applying the simplest Kochen-Specker set for quantum information processing, *Phys. Rev. Lett.* **113**, 090404 (2014).
 - [25] M. Arias, G. Cañas, E. S. Gómez, J. F. Barra, G. B. Xavier, G. Lima, V. D’Ambrosio, F. Baccari, F. Sciarrino, and

- A. Cabello, Testing noncontextuality inequalities that are building blocks of quantum correlations, *Phys. Rev. A* **92**, 032126 (2015).
- [26] G. Cañas, E. Acuña, J. Cariñe, J. F. Barra, E. S. Gómez, G. B. Xavier, G. Lima, and A. Cabello, Experimental demonstration of the connection between quantum contextuality and graph theory, *Phys. Rev. A* **94**, 012337 (2016).
- [27] M. Jerger, et al., Contextuality without nonlocality in a superconducting quantum system, *Nat Commun* **7**, 12930 (2016).
- [28] A. Crespi, M. Bentivegna, I. Pitsios, D. Rusca, D. Poderini, G. Carvacho, V. D'Ambrosio, A. Cabello, F. Sciarrino, and Roberto Osellame, Single-photon quantum contextuality on a chip, *ACS Photonics* **4**, 2807–2812 (2017).
- [29] Y. Xiao, Z.-P. Xu, Q. Li, H.-Y. Su, K. Sun, A. Cabello, J.-S. Xu, J.-L. Chen, C.-F. Li, and G.-C. Guo, Experimental test of quantum correlations from Platonic graphs, *Optica* **5**, 718–722 (2018).
- [30] Z.-H. Liu, H.-X. Meng, Z.-P. Xu, J. Zhou, S. Ye, Q. Li, K. Sun, H.-Y. Su, A. Cabello, J.-L. Chen, J.-S. Xu, C.-F. Li, and G.-C. Guo, Experimental observation of quantum contextuality beyond Bell nonlocality, *Phys. Rev. A* **100**, 042118 (2019).
- [31] W.-R. Qi, J. Zhou, L.-J. Kong, Z.-P. Xu, H.-X. Meng, R. Liu, Z.-X. Wang, C. Tu, Y. Li, A. Cabello, J.-L. Chen, and H.-T. Wang, Stronger Hardy-like proof of quantum contextuality, *Photon. Res.* **10**, 1582–1593 (2022).
- [32] S. Ru, W. Tang, Y. Wang, F. Wang, P. Zhang, and F. Li, Verification of Kochen-Specker-type quantum contextuality with a single photon, *Phys. Rev. A* **105**, 012428 (2022).
- [33] D. Qu, K. Wang, L. Xiao, X. Zhan, and P. Xue, State-independent test of quantum contextuality with either single photons or coherent light, *npj Quant. Inf.* **7**, 154 (2021).
- [34] K. Bharti, M. Ray, Z.-P. Xu, M. Hayashi, L.-C. Kwek, and A. Cabello, Graph-theoretic approach for self-testing in Bell scenarios, *PRX Quantum* **3**, 030344 (2022).